Cell Chemical Biology

Therapeutic potency of compound RMY-205 for pulmonary fibrosis induced by SARS-CoV-2 nucleocapsid protein

Graphical abstract
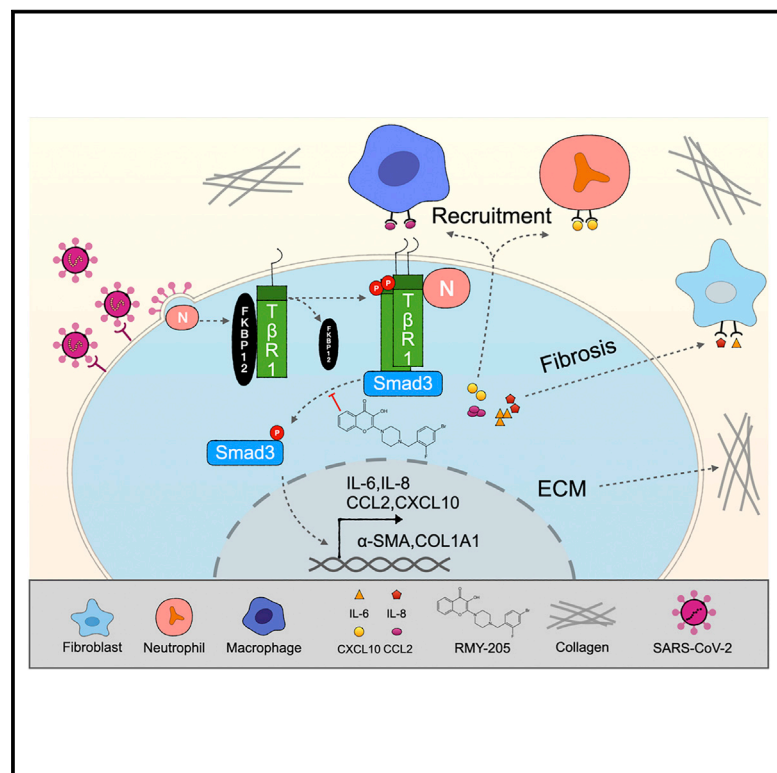
Authors

Zhi-yuan Zhang, Cui-yu Ju, Liu-zheng Wu, ..., Tianwei Lin, Fu-nan Li, Qiao Wu

Correspondence

twlin@xmu.edu.cn (T.L.), fnlee5@xmu.edu.cn (F.-n.L.), qiaow@xmu.edu.cn (Q.W.)

In brief

Pulmonary fibrosis is a typical sequela of COVID-19. Zhang et al. demonstrate that the nucleocapsid (N) protein of SARS-CoV-2 induces pulmonary fibrosis by activating TβRI-Smad signaling in lung fibroblasts. Furthermore, they identify a compound, RMY-205, that inhibits N protein-activated Smad3 and has good therapeutic potential for N protein-induced pulmonary fibrosis.

Highlights

- SARS-CoV-2-encoded N protein induces pulmonary fibrosis by activating lung fibroblasts

- N protein disrupts the interaction of TβRI-FKBP12 to activate TβRI-Smad signaling

- Compound RMY-205 binds to Smad3 to impair N protein-induced Smad3 activation

- RMY-205 has good therapeutic potential for pulmonary fibrosis induced by N protein

CellPress

Cell Chemical Biology

Article

Therapeutic potency of compound RMY-205 for pulmonary fibrosis induced by SARS-CoV-2 nucleocapsid protein

Zhi-yuan Zhang,[1,3] Cui-yu Ju,[1,3] Liu-zheng Wu,[1,3] Han Yan,[2,3] Wen-bin Hong,[1,3] Hang-zi Chen,[1] Peng-bo Yang,[1] Bao-Rui Wang,[2] Tong Gou,[2] Xiao-yan Chen,[1] Zhi-hong Jiang,[1] Wei-jia Wang,[1] Tianwei Lin,[1,*] Fu-nan Li,[2,*] and Qiao Wu[1,4,*]

[1]State Key Laboratory of Cellular Stress Biology, School of Life Sciences, Faculty of Medicine and Life Sciences, Xiamen University, Xiamen 361102, China
[2]Fujian Provincial Key Laboratory of Innovative Drug Target Research, School of Pharmaceutical Sciences, Xiamen University, Xiamen 361102, China
[3]These authors contributed equally
[4]Lead contact
*Correspondence: twlin@xmu.edu.cn (T.L.), fnlee5@xmu.edu.cn (F.-n.L.), qiaow@xmu.edu.cn (Q.W.)
https://doi.org/10.1016/j.chembiol.2023.02.004

SUMMARY

Pulmonary fibrosis is a typical sequela of coronavirus disease 2019 (COVID-19), which is linked with a poor prognosis for COVID-19 patients. However, the underlying mechanism of pulmonary fibrosis induced by severe acute respiratory syndrome coronavirus 2 (SARS-CoV-2) is unclear. Here, we demonstrated that the nucleocapsid (N) protein of SARS-CoV-2 induced pulmonary fibrosis by activating pulmonary fibroblasts. N protein interacted with the transforming growth factor β receptor I (TβRI), to disrupt the interaction of TβRI-FK506 Binding Protein12 (FKBP12), which led to activation of TβRI to phosphorylate Smad3 and boost expression of pro-fibrotic genes and secretion of cytokines to promote pulmonary fibrosis. Furthermore, we identified a compound, RMY-205, that bound to Smad3 to disrupt TβRI-induced Smad3 activation. The therapeutic potential of RMY-205 was strengthened in mouse models of N protein-induced pulmonary fibrosis. This study highlights a signaling pathway of pulmonary fibrosis induced by N protein and demonstrates a novel therapeutic strategy for treating pulmonary fibrosis by a compound targeting Smad3.

INTRODUCTION

Coronavirus is a single-stranded RNA virus that can infect vertebrates and cause respiratory, digestive, and nervous system diseases. Severe acute respiratory syndrome coronavirus 2 (SARS-CoV-2), identified in 2019, is a highly contagious infectious agent that causes significantly severe coronavirus disease 2019 (COVID-19) in human populations.[1,2] Although COVID-19 is a multi-system disease,[3] the lungs are the major infected organ, resulting in not only pneumonia but also pulmonary fibrosis.[4,5] It is reported that persistent fibrotic changes are observed in nearly 25% of the patients who recovered from severe COVID-19 a year after hospitalization,[6] and the degree of fibrosis correlates with the duration of the disease,[1] suggesting that pulmonary fibrosis is a frequent pulmonary sequela of COVID-19. Given the continued growth of the population of COVID-19 patients, it is of great urgency to develop new anti-fibrosis drugs for COVID-19-related complications.

SARS-CoV-2 has a genome of approximately 30,000 nt, encoding various structural, non-structural, and accessory proteins. Among the four structural proteins (spike [S] protein, envelope [E] protein, membrane [M] protein, and nucleocapsid [N] protein), N protein is one of the most abundant.[7] N protein is very stable, structurally conserved, and highly immunogenic and is considered a good clinical diagnostic marker and therapeutic target.[7] N protein undergoes liquid-liquid phase separation, which not only contributes to virion assembly, viral transcription, and replication[8,9] but is also considered to be a factor in its ability to inhibit interferon (IFN)-I signaling.[10] However, whether there is a direct connection between virus infection and pulmonary fibrosis and how virus infection changes the lung environment is still unclear in COVID-19.

Transforming growth factor β (TGF-β) plays a critical role in fibrosis diseases, including pulmonary fibrosis.[4] The canonical TGF-β signaling pathway is mainly dependent on the TβR-Smad signaling axis. TGF-β binds to its receptor, TGF-β receptor II (TβRII), which recruits TβRI molecules to form heterotetramers to activate TβRI kinase activity. The activated TβRI phosphorylates Smad2/3 and forms a complex with Smad4 to translocate to the nucleus, where they bind to the promoters of pro-fibrotic genes to initiate transcription of related genes, including α-smooth muscle actin (α-SMA) and collagen I, that promote fibrosis.[11]
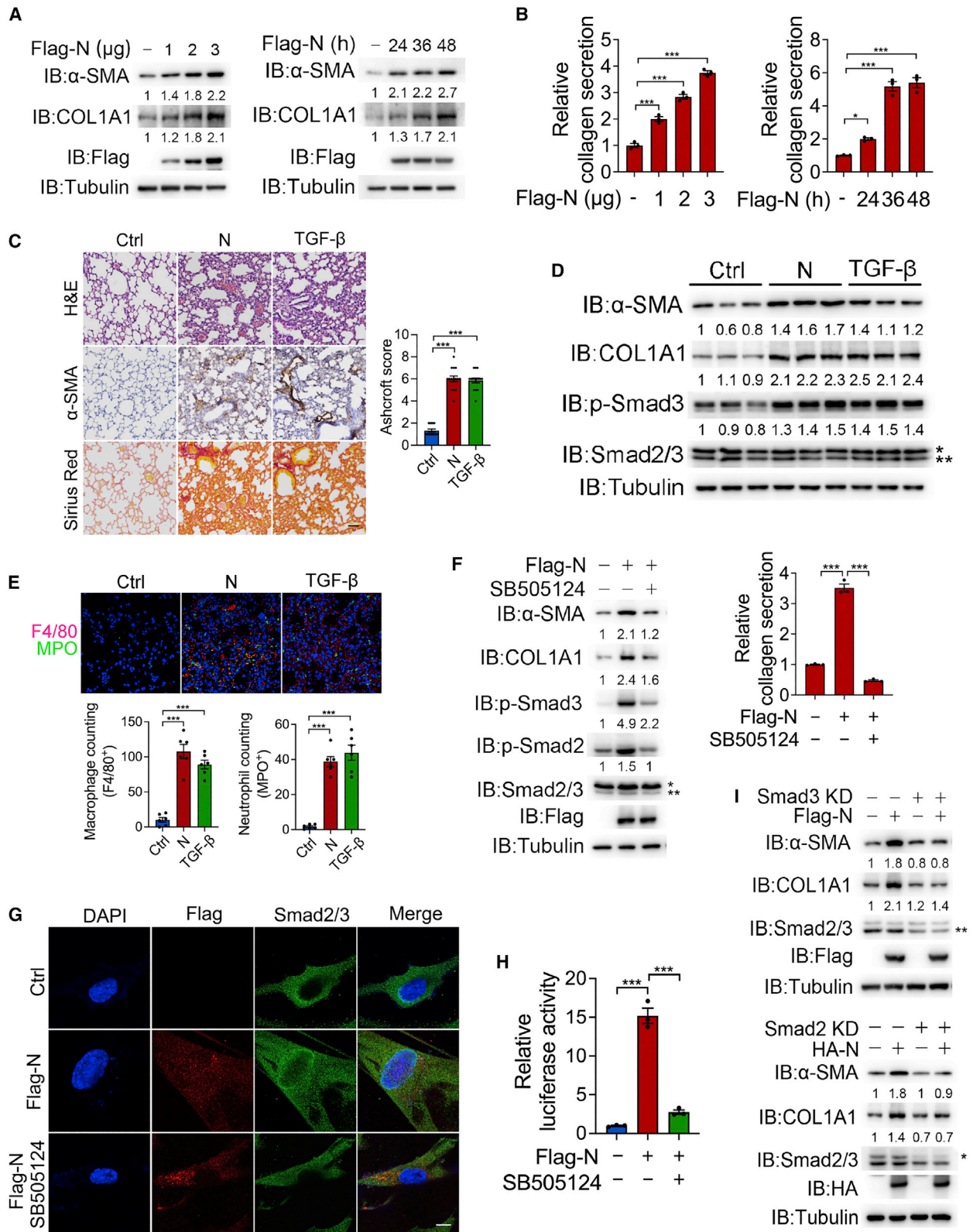
To date, there is still a lack of effective treatments for pulmonary fibrosis, especially that caused by SARS-CoV-2 infection. Therefore, unraveling the mechanism of SARS-CoV-2-induced pulmonary fibrosis and identification of new compounds for treating pulmonary fibrosis will be of great help to fight COVID-19. In the current study, we demonstrated that activation of the TGF-β signaling pathway by N protein of SARS-CoV-2 was responsible for the occurrence of pulmonary fibrosis. Moreover, a compound, RMY-205, was identified from our compound library that directly targeted Smad3 to block N protein-induced fibrosis in not only pulmonary fibroblasts but also mouse model of pulmonary fibrosis. The pharmacokinetic analysis showed the clinical potential of RMY-205. This study not only highlights a direct cause of SAR-CoV-2-associated pulmonary fibrosis but also demonstrates a novel therapeutic strategy for treating pulmonary fibrosis using RMY-205.

RESULTS

SARS-CoV-2 N protein induces pulmonary fibrosis

It has been shown that SARS-CoV-2 infection could induce pulmonary fibrosis through a variety of potential mechanisms, such as induction of pro-fibrotic macrophage responses.[12] The fact that the SARS-CoV-2 genome can be detected in lung fibroblasts upon SARS-CoV-2 infection[13] indicates that individual SARS-CoV-2 proteins might play a role in lung fibroblasts during pulmonary fibrosis. Here we showed that, after transfection of different SARS-CoV-2 structural and non-structural proteins in lung fibroblast HFL-1 cells, SARS-CoV-2-encoded N protein was the sole protein that induced fibrosis with the elevation of α-SMA expression levels (Figure S1A), a typical marker of fibrosis,[14] in a dose- and time-dependent fashion (Figure 1A). Pulmonary fibrosis is closely associated with deposition of extracellular matrix (ECM) proteins, especially collagen.[15] Increased expression of collagen type I α1 (COL1A1) and secretion of collagen proteins were clearly demonstrable when N protein was expressed in HFL-1 cells (Figures 1A and 1B), which suggests that N protein could directly activate lung fibroblasts in a cell-autonomous manner for pulmonary fibrosis.

To gain insight into N protein function *in vivo*, C57BL/6 mice were intranasally exposed to an adeno-associated virus (AAV) encoding N protein to induce pulmonary fibrosis.[16] After 30 days, pulmonary fibrosis was distinctly detectable with alveolar septal thickening (indicated by Hematoxylin-Eosin [H&E] staining), enhanced α-SMA expression (indicated by immunohistochemistry [IHC] and western blotting), and collagen deposition (indicated by Sirius red staining and western blotting) (Figures 1C and 1D). Ashcroft scoring, a widely used method to quantify pulmonary fibrosis,[17] also revealed severe pulmonary fibrosis induced by N protein (Figure 1C, right). This N protein-induced pulmonary fibrosis was accompanied by recruitment of myeloid cells, including macrophages and neutrophils (indicated by F4/80- or myeloperoxidase [MPO]+ cells respectively) (Figure 1E). All of these results consistently indicate that N protein could activate lung fibroblasts to induce pulmonary fibrosis.

The pro-fibrotic effects of N protein were comparable with that of TGF-β, one of the most potent fibrogenic factors, detected *in vivo* in mouse samples (Figures 1C and 1E). Upon TGF-β stimulation, phosphorylation of Smad2/3 was elevated, leading to activation of the TGF-β/Smad signaling pathway following activation of fibroblasts (Figure S1B).[11] Similar to TGF-β, expression of N protein also markedly increased the phosphorylation of Smad2 and Smad3 in mouse samples (Figure 1D) and HFL-1 cells (Figure 1F), leading to their nuclear translocation (Figure 1G), and activation of Smad transactivation activity (Figure 1H). When TGF-β signaling was suppressed by SB505124, a selective inhibitor of TβRI, N protein not only lost its ability to induce Smad phosphorylation, nuclear translocation, and transactivation activity, but it also failed to elevate the expression of α-SMA and COL1A1 (Figures 1F–1H). These results indicated that activation of TGF-β/Smad signaling was required for the pro-fibrotic function of N protein. To verify this, Smad2 and Smad3 were knocked down in HFL-1 cells. Under this condition, N protein could barely induce expressions of α-SMA and COL1A1 (Figure 1I). Collectively, it can be concluded that N protein activates the TGF-β/Smad signaling pathway to activate lung fibroblasts with the subsequent induction of pulmonary fibrosis.

N protein interacts with TβRI to activate its phosphorylation

The underlying mechanism for N protein-activated TGF-β/Smad signaling was further investigated. It could be shown that only TβRI, but not any other members of the TGF-β/Smad signaling pathway, including TβRII, Smad2, and Smad3, could interact with N protein in HFL-1 cells (Figure 2A), indicating that N protein might activate TGF-β/Smad signaling through regulation of TβRI. Upon TGF-β stimulation, TβRII phosphorylates TβRI to activate TGF-β/Smad signaling.[18] We also found that N protein induced phosphorylation of TβRI in a dose-dependent manner (Figure 2B), leading to enhancement of TβRI interaction with, and subsequent phosphorylation of, Smad2 or Smad3 (Figures 2C,

Figure 1. N protein induces pulmonary fibrosis

N protein (2 μg) was transfected into HFL-1 cells for 36 h, and the cells were collected for analysis unless specified otherwise.

(A and B) N proteins were expressed at the indicated times and doses for detection of α-SMA and COL1A1 expression (A) and collagen secretion in cultured medium (B).

(C–E) In the N protein-induced pulmonary fibrosis mouse model (n = 6 independent mice), α-SMA expression and collagen deposition (Sirius red staining) (scale bar, 100 μm) (C, left), and Ashcroft score (C, right) were evaluated in lung sections. The infiltration of macrophages (F4/80+ staining) and neutrophils (MPO+ staining) (E, top) was detected and quantified (E, bottom). In the same samples, western blots were performed (D; *, Smad2, **, Smad3). TGF-β was used as a positive control.

(F–H) Cells expressing N protein were treated with SB505124 (10 μM, 24 h). α-SMA and COL1A1 expression, Smad2/3 phosphorylation (F, left) and collagen secretion (F, right) were detected, and Smad2/3 localization (scale bar, 10 μm) (G) and transcription activities (H) were detected.

(I) In Smad2 or Smad3 knockdown cells, N protein was overexpressed, and western blots were performed.

The intensities of Western Blot bands relative to the loading control (such as Tubulin) were quantified and shown under each band. Statistical data are presented as the mean ± SEM. The differences between multiple groups were analyzed by using one-way ANOVA. *p < 0.05; **p < 0.01; ***p < 0.001; ns, not significant.
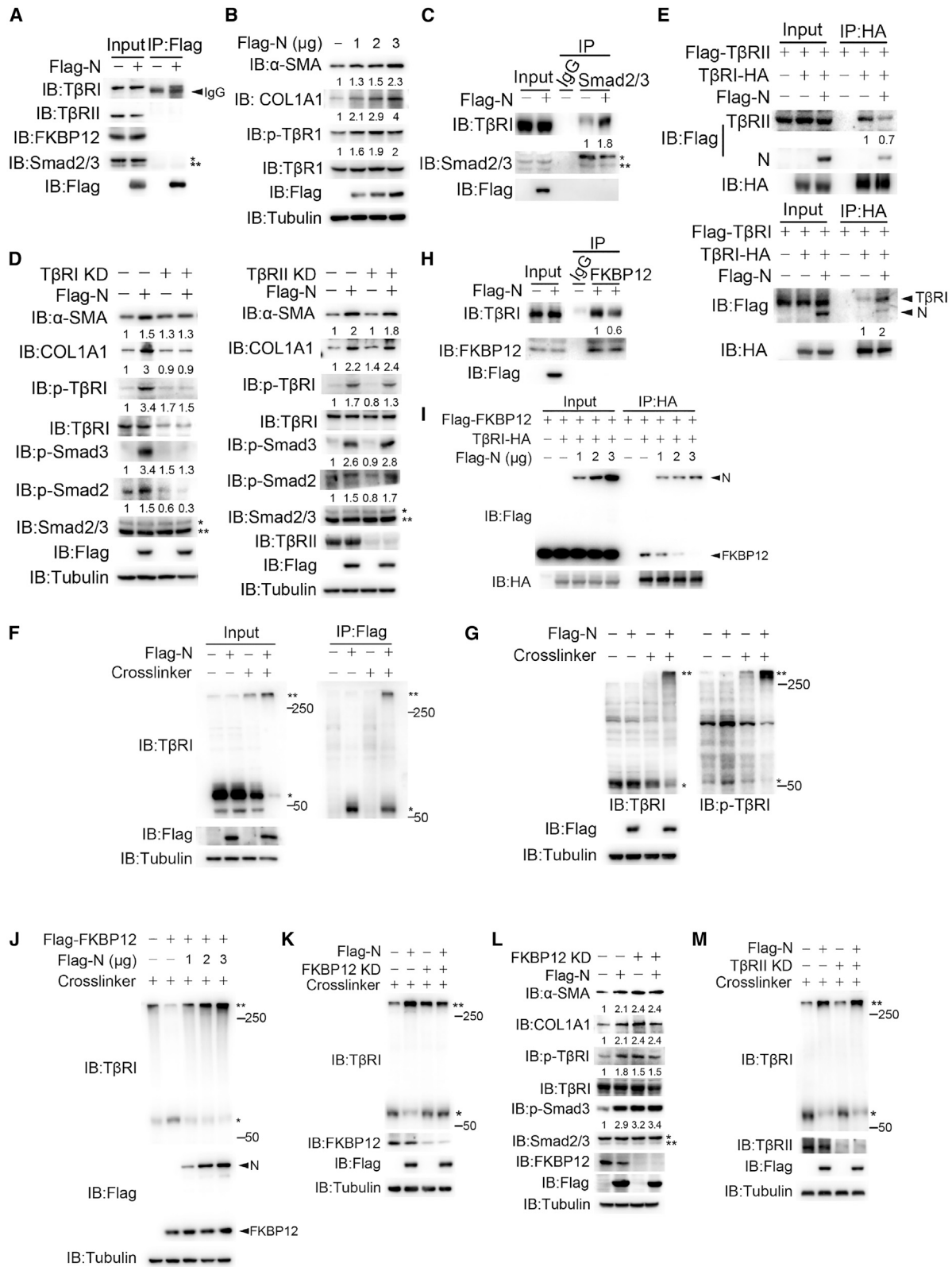
Figure 2. N protein binds TβRI to activate TGF-β/Smad signaling

N protein (2 μg) was transfected into HFL-1 cells for 36 h, unless specified otherwise.

(A) Interactions between N protein and endogenous TβRI, TβRII, FKBP12, or Smad2/3.

S2A, and 2D, left) to boost the expression of α-SMA and COL1A1 (Figures 2B and 2D). When TβRI was knocked down in HFL-1 cells, N protein lost its ability to stimulate Smad2/3 phosphorylation as well as α-SMA and COL1A1 expression (Figure 2D, left). In contrast, knockdown of TβRII influenced neither N protein-induced phosphorylation of TβRI and Smad2/3 nor α-SMA and COL1A1 expression (Figure 2D, right). These results suggest that N protein activates TGF-β/Smad signaling in a TβRI- but not TβRII-dependent manner, which is different from classic activation of TGF-β/Smad signaling by its native ligand TGF-β.

N protein interfered with the interaction between TβRI and TβRII (Figure 2E, left) but strengthened the TβRI-TβRI interaction (Figure 2E, right), leading to TβRI polymerization (Figures 2F and S2B). This TβRI polymerization was closely associated with activation of TβRI because N protein-induced TβRI phosphorylation was associated with formation of TβRI polymers (Figures 2G and S2C). While the TβRI inhibitor SB505124 could block N protein-induced TβRI phosphorylation, it could not prevent N protein-induced TβRI polymerization (Figure S2D), suggesting that TβRI polymerization occurred before its phosphorylation. Given that N protein interacted with the TβRI polymer (Figures 2F and S2B), it is likely that the interaction of N protein promotes polymerization of TβRI, leading to self-phosphorylation and activation of TβRI.

It has been reported that the upstream factor FKBP12 binds and stabilizes TβRI in its inactive form,[19] and disruption of the TβRI-FKBP12 interaction leads to polymerization and phosphorylation of TβRI in a TβRII-independent manner.[20] Although N protein did not interact with endogenous FKBP12 in HFL-1 cells (Figure 2A), it did interfere with the endogenous interaction between FKBP12 and TβRI (Figure 2H). This may be due to the competition between N protein and FKBP12 for binding to TβRI. In the absence of N protein, the interaction between FKBP12 and TβRI was evident. In contrast, the increased expression of N protein suppressed the interaction between FKBP12 and TβRI and enhanced the interaction between TβRI and N protein (Figure 2I). So, N protein abolished the inhibitory effect of FKBP12 on polymerization of TβRI, enhancing formation of the TβRI polymer (Figure 2J). When FKBP12 was knocked down, polymerization and phosphorylation of TβRI were elevated. Consequently, N protein could not promote any additional polymerization or phosphorylation of TβRI and not induce expression of α-SMA and COL1A1 (Figures 2K and 2L). In contrast, knockdown of TβRII had no effect on N protein-induced TβRI polymerization (Figure 2M), phosphorylation of TβRI, and expressions of α-SMA and COL1A1 (Figure 2D, right),

indicating that it was the substitution of N protein for FKBP12 in the interaction with TβRI that resulted in polymerization and activation of TβRI in a TβRII-independent manner. Together, these results demonstrate that the interaction of N protein with TβRI competitively disrupted the TβR1-FKBP12 association to relieve FKBP12-suppressed TβRI polymerization and self-phosphorylation in a TβRII-independent manner, which led to activation of TGF-β/Smad signaling to boost α-SMA and COL1A1 expression and induction of pulmonary fibrosis.

Compound RMY-205 targets Smad3 to interfere N protein-enhanced Smad3-TβRI interaction

A house compound library was screened for small molecules that could attenuate the N protein-elevated α-SMA expression. A compound named RMY-205 (2-(4-(4-bromo-2-fluorobenzyl) piperazin-1-yl)-3-hydroxy-4H-chromen-4-one) was identified (Figure 3A) that had the ability to downregulate N protein-induced α-SMA and COL1A1 expression levels and collagen secretion in a time- and dose-dependent manner in HFL-1 cells (Figure 3B). Immunofluorescence staining also indicated that RMY-205 could suppress N protein-induced α-SMA expression (Figure 3C). Furthermore, RMY-205 effectively inhibited TGF-β-induced Smad3 phosphorylation and α-SMA and COL1A1 expression in HFL-1 cells (human lung fibroblasts) as well as in AC16 (human cardiomyocytes), LX-2 (human hepatic stellate cells), and human primary dermal cells (Figure S3A). Therefore, it is likely that RMY-205 can function as an inhibitor of TGF-β/Smad signaling in multiple cell lines.

RMY-205 did not interfere with the interactions between N protein and TβRI, TβRI and TβRII (Figure S3B), or TβRI and FKBP12 (Figure S3C). N protein-induced TβRI polymerization was not influenced by RMY-205 either (Figure S3D). However, RMY-205 could attenuate the N protein-induced TβRI interaction with Smad3, but not with Smad2, in exogenous co-immunoprecipitation (Co-IP) (Figure S3E) and endogenous coIP assays (Figure 3D) as well as the glutathione S-transferase (GST) pull-down assay in vitro (Figure S3F). This specific interference resulted in RMY-205 inhibition of N protein-induced phosphorylation of Smad3 but not of Smad2 (Figure 3E), excluding Smad2 playing a role in this RMY-205 function. It is an indication that RMY-205 interfered with the interaction between TβRI and Smad3 rather than that between N protein and TβRI.

To determine whether RMY-205 could directly bind to either TβRI or Smad3, we carried out an isothermal titration calorimetry (ITC) assay and found that RMY-205 was a binder to Smad3 with a K_d value of 8 μM (Figure 3F) but not to either Smad2 or TβRI

(B) Effect of N protein on α-SMA and COL1A1 expression and TβRI (T204) phosphorylation.
(C) Effect of N protein on the interaction between endogenous TβRI and Smad2/3.
(D) TβRI (left) and TβRII (right) were knocked down first, and the N proteins were expressed. α-SMA and COL1A1 expression and phosphorylation level of TβRI and Smad2/3 were detected.
(E) Different plasmids were transfected into cells, and the interaction of TβRI-TβRII (top) and TβRI-TβRI (bottom) was detected.
(F and G) N protein was expressed in cells, and polymerization of TβRI was determined (*, monomer TβRI; **, polymer TβRI). The interaction of N protein with TβRI polymer (F) and phosphorylation of TβRI polymer (G) are shown.
(H) Effect of N protein on the endogenous TβRI-FKBP12 interaction.
(I) Indication of competition between N protein and FKBP12 binding to TβRI.
(J and K) N protein-induced TβRI polymerization was detected in FKBP12-overexpressing (J) or knockdown (K) HEK293T cells.
(L) Effects of N protein on α-SMA expression and phosphorylation levels of TβRI and Smad2/3 in FKBP12 knockdown HFL-1 cells.
(M) N protein-induced TβRI polymerization was determined in TβRII knockdown HEK293T cells.
The intensities of Western Blot bands relative to the loading control (such as Tubulin) were quantified and shown under each band.
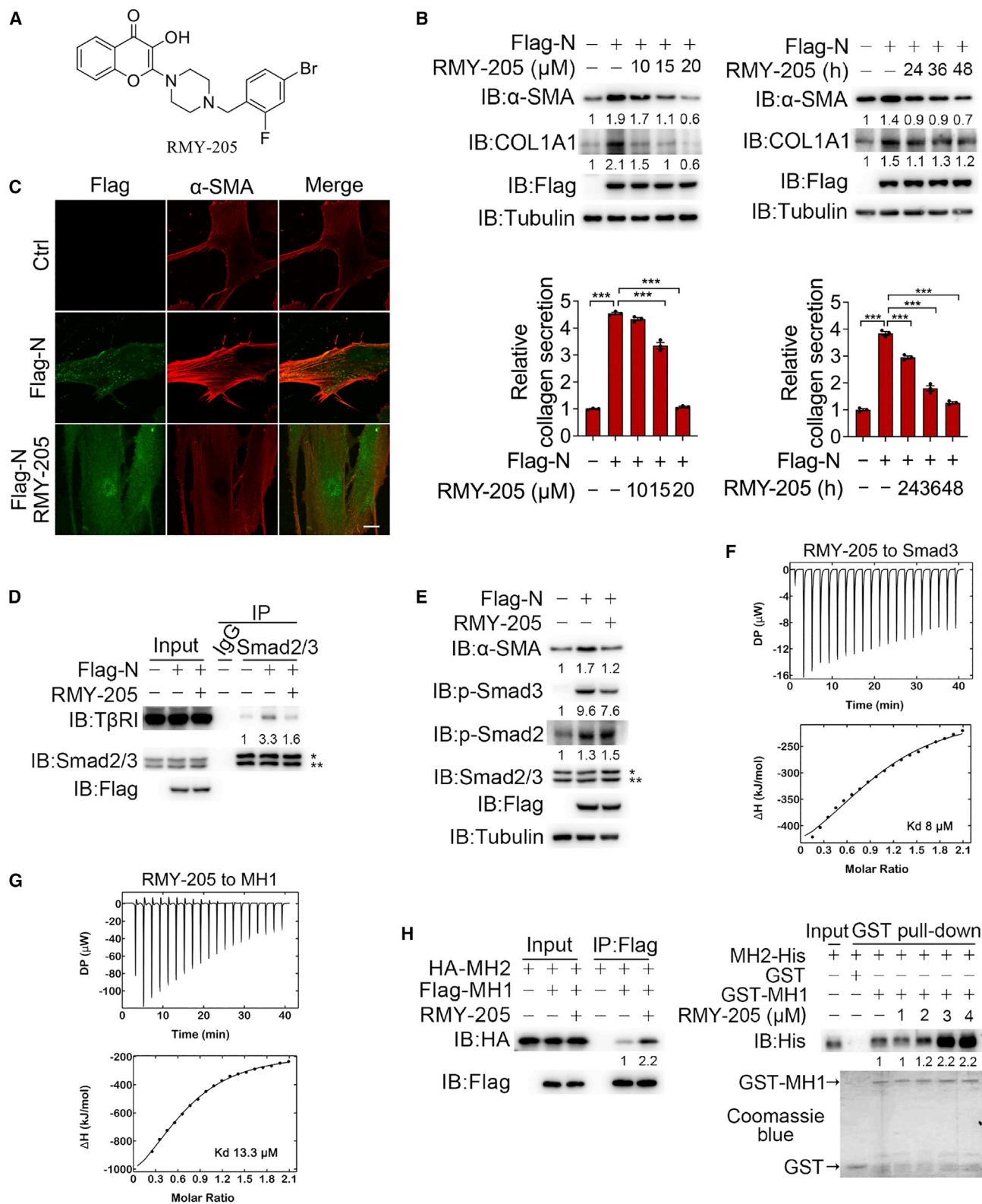
Figure 3. RMY-205 targets Smad3 to interfere with the N protein-enhanced Smad3-TβRI interaction

N protein (2 μg) was transfected into HFL-1 cells overnight, and the cells were treated with RMY-205 (20 μM) for 24 h for confocal microscopy or 36 h for western blotting, unless specified otherwise.

(A) The structure of compound RMY-205.

(Figures S3G and S3H). By separately expressing the individual domains of Mad Homology 1 (MH1) and MH2 of Smad3 (Figure S3I), it was found that MH1, but not MH2 (Figure S3J), was the binding domain to RMY-205 (Figure 3G; the K_d value is 13.3 μM). MH1 is a critical domain required for DNA binding, and MH2 is the domain for the interaction with TβRI.[21] RMY-205 was not to directly interfere with the interaction between Smad3 and TβRI but to substantially enhance the interaction between MH1 and MH2 domains (Figure 3H). Given that the MH1 and MH2 domains physically interact with each other, resulting in suppression of each other's function,[22] it is possible that the binding of RMY-205 to Smad3 may reinforce the MH1-MH2 interaction within the Smad3 protein to exclude the N protein-induced TβRI binding with Smad3, leading to failure of TβRI to phosphorylate Smad3.

The binding and subsequent suppression of Smad3 by RMY-205 suggested that RMY-205 was an inhibitor of Smad3. (E)-SIS3 is an inhibitor of Smad3 in myofibroblast differentiation of fibroblasts by TGF-β1.[23] Inhibition of TGF-β-induced Smad3 phosphorylation and α-SMA expression by RMY-205 was comparable with that by (E)-SIS3 (Figure S3K, left). However, no inhibitory effect of (E)-SIS3 toward N protein-induced Smad3 activation could be shown (Figure S3K, right), implying a context-dependent function of (E)-SIS3. Nocodazole has been reported to activate Smad3 in an Mps1- but not TβRI-dependent manner.[24] RMY-205 also inhibited nocodazole-induced Smad3 phosphorylation in HFL-1, LX-2, and AC-16 cells (Figure S3L).

Lys41 of Smad3 is critical for RMY-205 binding

Molecular docking was employed to analyze the critical sites in the MH1 domain of Smad3 for RMY-205 binding. As shown in Figure 4A, the best model for the RMY-205–MH1 complex was to occupy the DNA-binding pocket formed by the H2 helix and B2 and B3 strands. In this model, the important interaction includes a cation-π interaction between MH1 Lys41 and the benzene ring of RMY-205 and a hydrogen bond between MH1 Ser37 and the enolic hydroxyl group of RMY-205 (Figure 4A). To rationalize the role played by RMY-205, an MH1-MH2 interaction model was created by docking the two domains with Rosetta. The model indicated that the RMY-205 binding site was right at the interface between the MH1 and MH2 domains (Figure S4A). So it seems that RMY-205 binding strengthens the protein-protein interaction between the MH1 and MH2 domains, which, in turn, results in steric hindrance to block TβRI binding (Figure S4B).

Because Ser37 and Lys41 of Smad3 likely critical for RMY-205 binding, as shown in the docking model, we made two points mutants, MH1[S37A] and MH1[K41A], for analysis. Although mutation of S37A nor K41A did not influence the interaction between MH1 and MH2, RMY-205 enhanced the interaction of

MH2 with either MH1 or MH1[S37A], but enhancement of the interaction was abolished with MH1[K41A] in GST pull-down (Figure 4B) and coIP assays (Figure 4C), indicating that MH1 Lys41 is required for RMY-205 function. When Lys41 was mutated to Ala in full-length Smad3 (Smad3[K41A]), the interaction between TβRI and Smad3 was not impaired (Figure 4D), but RMY-205 could no longer dampen the interaction between Smad3[K41A] and TβRI compared with the Smad3-TβRI interaction (Figure 4E). In HFL-1 cells with Smad3 knocked down, re-expression of Smad3[K41A] led to loss of RMY-205 influence on N protein-induced α-SMA expression (Figure 4F), probably because of failure of RMY-205 binding to Smad3[K41A] (Figure S4C). Evidently, Lys41 in Smad3 is critical for RMY-205 binding.

RMY-205 inhibits secretion of cytokines by suppressing TGF-β/Smad3 signaling

Smad2/3 are transcription factors, and their translocation from the cytosol to the nucleus could activate the TGF-β/Smad signaling pathway.[25] Smad2/3 proteins were in the cytosol of HFL-1 cells but would translocate to the nucleus with introduction of N protein (Figure 5A). Treatment with the TβRI inhibitor SB505124 caused Smad2/3 proteins to remain in the cytosol even in the presence of N protein. Like SB505124, RMY-205 also blocked N protein-induced Smad2/3 nuclear translocation (Figure 5A). This RMY-205-inhibited Smad2/3 translocation could also be shown in a fractionation assay of HFL-1 cells (Figure 5B). As a result, RMY-205 inhibited the N protein-induced transactivation activity of Smad in a Smad3-dependent manner (Figure 5C, top), which was abolished by Smad3[K41A] (Figure 5C, bottom). Clearly, RMY-205 can suppress N protein-induced pulmonary fibrosis through TGF-β/Smad3 signaling.

Because pulmonary fibrosis is usually accompanied by inflammation,[15] and N protein-induced pulmonary fibrosis was accompanied by infiltration of inflammatory cells (Figure 1E), it is possible that expression of N protein may stimulate secretion of cytokines from lung fibroblasts. A human cytokine antibody array was employed to detect N protein-induced cytokine secretion in HFL-1 cells. The results showed that expression of N protein markedly enhanced secretions of C-C Motif Chemokine 2 (CCL2), C-X-C Motif Chemokine 10 (CXCL10), interleukin-6 (IL-6), and IL-8 (Figure S5A). An enhancing effect of N protein on the mRNA levels of these cytokines was also observed (Figure S5B). However, when TβRI was knocked down in HFL-1 cells, N protein lost its ability to elevate the mRNA levels in these cytokines (Figure S5B), suggesting that N protein may stimulate the expression of these cytokines through activation of Smad downstream targets. This finding was supported by analysis of chromatin IP sequencing (ChIP-seq) data in the public domain, where Smad2/Smad3 have

---

(B) Cells were treated with RMY-205 at the indicated times or doses, and the expression levels of α-SMA and COL1A1 (top) and collagen secretion (bottom) were determined.

(C) α-SMA expression was determined with or without RMY-205 treatment (scale bar, 10 μm).

(D and E) Cells expressing N protein were treated with RMY-205, and the interactions between endogenous TβRI and Smad2/3 (D), and α-SMA expression and Smad2/3 phosphorylation (E) were determined.

(F and G) RMY-205 binding to Smad3 (F) or the MH1 domain of Smad3 (G).

(H) The effect of RMY-205 on the MH1-MH2 interaction, detected by coIP assay (left) or GST pull-down assay (right).

The intensities of Western Blot bands relative to the loading control (such as Tubulin) were quantified and shown under each band. Statistical data are presented as the mean ± SEM. The differences between multiple groups were analyzed by using one-way ANOVA. *p < 0.05; **p < 0.01; ***p < 0.001; ns, not significant.
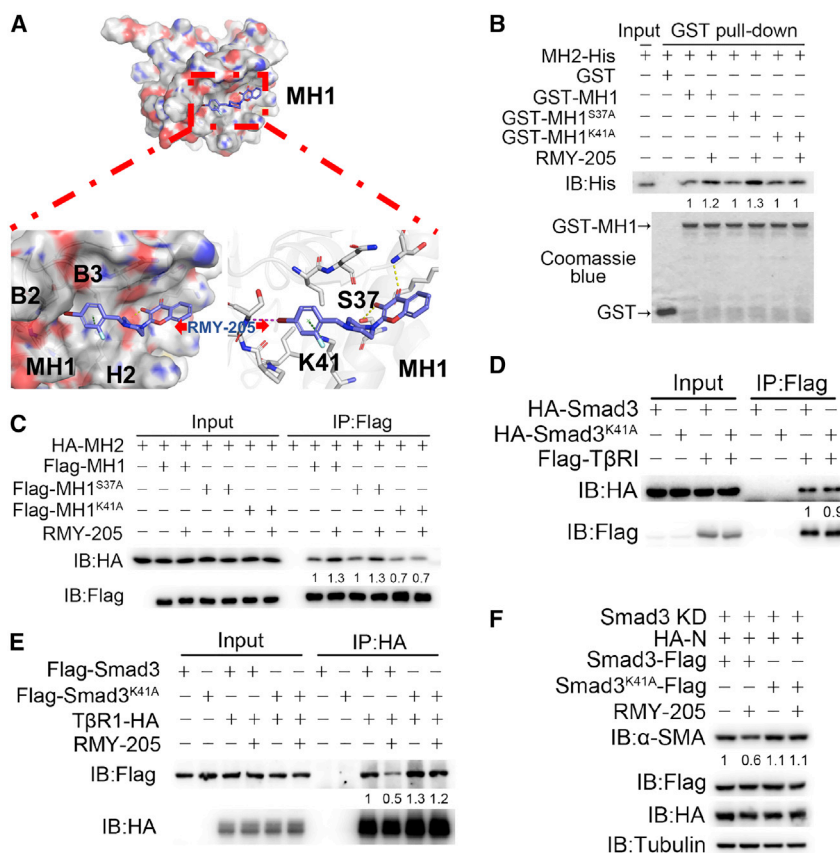
Evaluation of RMY-205 in an N protein-induced mouse model of pulmonary fibrosis

To further delineate the role of RMY-205, an N protein-induced mouse model of pulmonary fibrosis was employed. RMY-205 suppression of fibrosis of primary mouse pulmonary fibroblasts was first investigated. The mRNA expression levels of CCL2, CXCL10, and IL-6 (IL-8 is not expressed in mice) were upregulated by N protein in a TβR1-dependent manner in primary mouse pulmonary fibroblasts (Figure S6A), consistent with the data derived from human lung fibroblasts HFL-1 cells, and RMY-205 significantly inhibited N protein-induced α-SMA and COL1A1 expression (Figure 6A) with suppression of the N protein-elevated mRNA of CCL2, CXCL10, and IL-6 expression (Figure 6B) and their release levels (Figure 6C). In addition, expression of N protein in mouse primary lung fibroblasts promoted recruitment of primary bone marrow-derived macrophages (BMDMs) and primary neutrophils, which were abolished by the RMY-205 treatment (Figure 6D). Clearly, RMY-205 could suppress N protein-induced fibrosis in primary mouse pulmonary fibroblasts to impair the recruitment of inflammatory cells.

In the mouse model of pulmonary fibrosis induced by N protein encoded in an AAV, alveolar septal thickening was observed in lung sections, accompanied by α-SMA expression and collagen deposition. Administration of RMY-205 (10 mg/kg) to mice weekly for 30 days alleviated alveolar septal thickening and decreased α-SMA expression and collagen deposition (Figure 6E), which was closely associated with suppression of N protein-induced phosphorylation of Smad3 (Figure 6F). Moreover, RMY-205 also markedly attenuated N protein-promoted infiltration of macrophages and neutrophils in the lung tissue (Figure 6G) with suppression of N protein-induced secretion of CCL2, CXCL10, and IL-6 in bronchoalveolar lavage fluid

the potential to bind to the promoters of these cytokine genes (Figure S5C). CCL2 and CXCL10 participate in recruitment of inflammatory cells,[26,27] and overexpression of N protein in HFL-1 cells substantially promoted recruitment of THP1 macrophages and differentiated HL60 neutrophils. When CCL2 or CXCL10 was knocked down, N protein lost these functions (Figure S5D), indicating that N protein-activated lung fibroblasts may facilitate remodeling of the inflammatory lung microenvironment through recruitment of inflammatory cells. Elevation of IL-6 and IL-8 levels was commonly observed in severe COVID-19 patients.[28] When IL-6 and IL-8 secreted from HFL-1 cells were neutralized by their corresponding antibodies, the pro-fibrotic effect of N protein, indicated by α-SMA expression, was impaired (Figure S5E). Hence, N protein activation of lung fibroblasts can lead to IL-6 and IL-8 secretion to create a feedforward loop that further exacerbates pulmonary fibrosis.

RMY-205's inhibitory functions on N protein-induced cytokine secretion were further investigated. When HLF-1 cells were treated with RMY-205, the N protein-induced mRNA expression of IL6, IL8, CCL2, and CXCL10 was downregulated (Figure 5D), consistent with the data showing that RMY-205 inhibited Smad3 binding to the promoters of genes of these cytokines in the ChIP analysis (Figure 5E). As a result, RMY-205 led to attenuation of recruiting THP1 macrophages and differentiated HL60 neutrophils by N protein (Figure 5F). All of these results consistently demonstrate that RMY-205 not only inhibits N protein-induced activation of lung fibroblasts but also interdicts secretion of cytokines to alleviate the inflammatory storm.
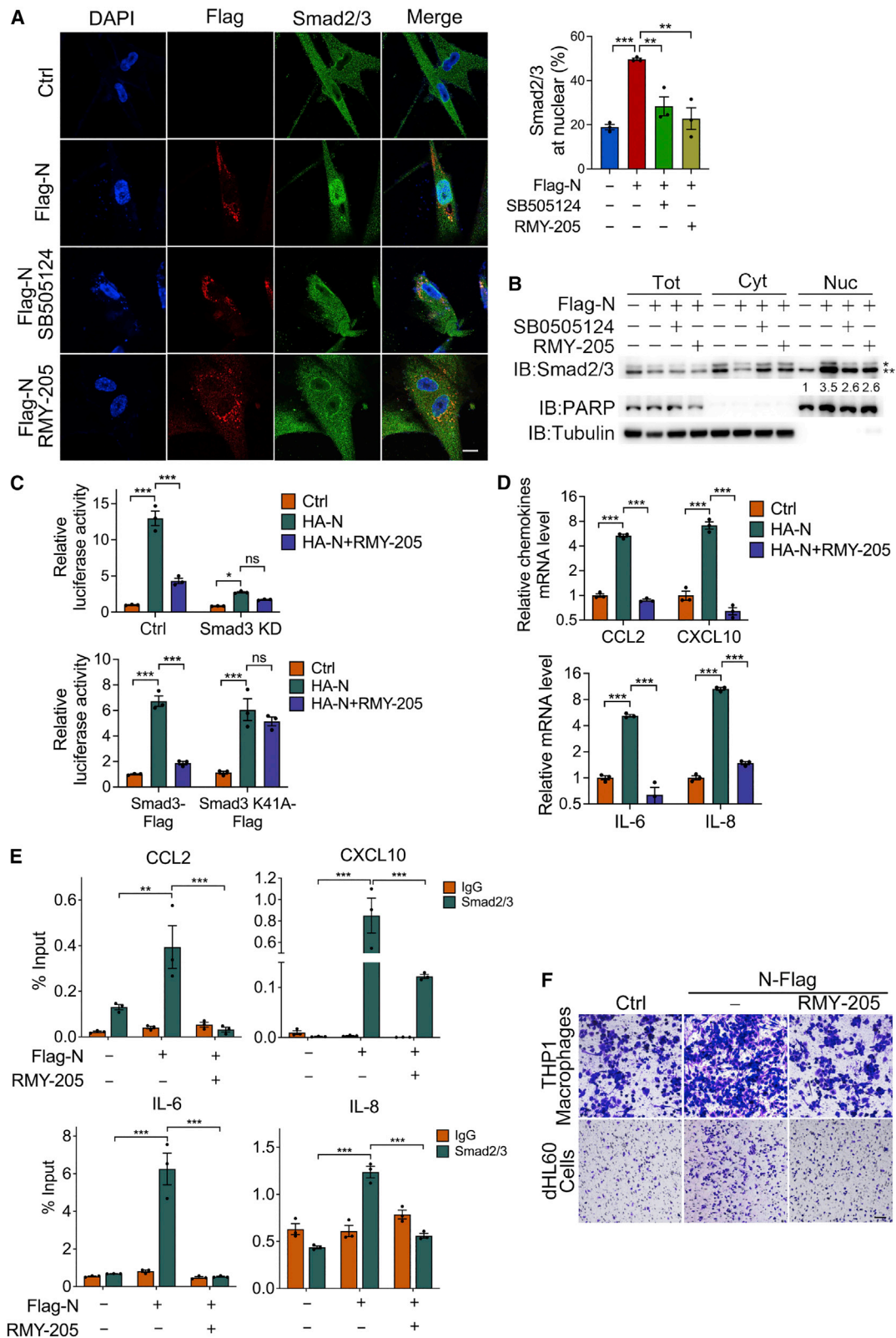
Figure 5. RMY-205 inhibits cytokine secretion via Smad3
Different plasmids were transfected into HFL-1 cells overnight, and the cells were treated with RMY-205 (20 µM) for 24 h for confocal microscopy or 36 h for western blot unless specified otherwise.

(Figure 6H). Therefore, RMY-205 is effective in alleviating N protein-induced pulmonary fibrosis and inflammation in the mouse model through inhibiting Smad3 activation.

Because TGF-β/Smad signaling is a master pathway for regulation of tissue fibrosis, it is possible that RMY-205 may broadly suppress fibrosis in different tissues. To this end, we used an Adriamycin-induced renal fibrosis mouse model. Adriamycin is reported to be able to activate TGF-β/Smad signaling,[29] and RMY-205 could effectively alleviate renal fibrosis with suppressed Smad3 phosphorylation and COL1A1 expression induced by Adriamycin in the mouse model (Figure S6B), indicating a broader function of RMY-205 in suppression of tissue fibrosis.

During RMY-205 administration, the weight of the mice and of various organs (including the heart, liver, spleen, lungs, and kidneys) were not significantly changed (Figure S6C). An RMY-205 pharmacokinetic (PK) analysis (intravenous [i.v.] 2 mg/kg, per os [p.o.] 10 mg/kg, and intraperitoneal [i.p.] 10 mg/kg) in mice was carried out. The key PK parameters of RMY-205 are summarized in Table 1. When RMY-205 was used separately through the i.v., i.p., or oral routes, it was with area under the curve (AUC) values of 995, 2,129, and 1,871 ng h/mL, respectively. After p.o. administration, RMY-205 showed a half-life ($T_{1/2}$) of 2.55 h, bioavailability of 37.6%, and clearance (CL) rate of 34 mL/min/kg. These favorable PK properties, especially with an oral bioavailability of 37.6%, demonstrated the potential of RMY-205 as an oral drug.

RMY-205 is effective for inhibiting pulmonary fibrosis induced by N protein of different SARS-CoV-2 variants

Different SARS-CoV-2 variants are emerging in the COVID-19 pandemic. To determine whether N protein from different SARS-CoV-2 variants also induced pulmonary fibrosis, plasmids encoding N protein from the Alpha, Beta, Gamma, Delta, and Omicron variants of SARS-CoV-2 were made for transfection in HFL-1 cells. These N proteins from the SARS-CoV-2 variants could similarly induce the expression levels of α-SMA and COL1A1 and phosphorylation level of Smad3 (Figure 7A). Smad3 phosphorylation induced by these N protein variants could be abolished by RMY-205 (Figure 7B), which led to suppression of α-SMA and COL1A1 expression (Figure 7B). Although the expression and secretion of CCL2, CXCL10, and IL-6 varied in mouse primary pulmonary fibroblasts induced by different N proteins, RMY-205's suppressive role was similar for all of these N protein variants (Figures S7A and S7B), further demonstrating a common effect of RMY-205 in antagonizing N protein-induced pulmonary fibrosis.

Additional experiments were carried out on the N protein of the Omicron variant, the currently dominant variant.[30] Intranasal expo-

sure of the AAV encoding N protein of the Omicron variant induced the typical phenotype of pulmonary fibrosis in mice, with alveolar septal thickening, collagen deposition (Figure 7C), elevation of Smad3 phosphorylation, α-SMA and COL1A1 expression (Figure 7D), and infiltration of macrophages and neutrophils (Figure 7E). Again, RMY-205 effectively suppressed these pro-fibrotic effects of N protein of the Omicron variant (Figures 7C–7E), indicating that RMY-205 can antagonize SARS-CoV-2-induced pulmonary fibrosis in vivo for SARS-CoV-2 variants.

Finally, we carried out a structure-activity relationship (SAR) analysis of RMY-205 with 16 derivatives. These compounds showed different effects on N protein-induced expression levels of α-SMA (Figure 7F). As summarized in Table 2, when the R_1 position was the F or Br group (WBR-1, WBR-2, WBR-5, or WBR-6), the overall inhibitory effect of the compound on α-SMA was low. When the R_1 position was the H group and the benzene ring was modified in one position, the biological activity of the compounds with ortho-substitution on the benzene ring (RMY-188, RMY-183 or WBR-14) was very low. However, the activity could be improved in the meta-substitution, but only with the group of Cl (WBR-12). The para-substitution of Br (RMY-190) had the highest activity. When the benzene ring was with double substitutions, those 2,6-substituted and 2,4-substituted compounds had high inhibitory activity on α-SMA. Together, these data indicated that the inhibition of RMY compounds on α-SMA could be improved by keeping the H group at the R_1 position and substituting the benzene ring at 2,4 positions (RMY-195 or RMY-205) in addition to the para-substitution of Br (RMY-190). Furthermore, compared with RMY-205 (median effect concentration [EC50] = 2.99 μM), the EC_{50} of RMY-190 is better (EC_{50} = 2.01 μM), and the EC_{50} of RMY-195 is almost similar (EC_{50} = 3.27 μM) (Figure 7G). Together, these results indicate that RMY-190 and RMY-195 are also promising compounds. Surely, the binding modes of RMY-195 and RMY-90 with Smad3 and their biological functions deserve further investigation.

DISCUSSION

Pulmonary fibrosis is a well-recognized sequela of acute respiratory distress syndrome (ARDS).[31] Although ARDS is the most frequent complication of severe COVID-19, it was still not clear how SARS-CoV-2 infection induces pulmonary fibrosis. A recent single-cell transcriptomic study indicated that SARS-CoV-2 infection triggers pro-fibrotic responses of CD163+ macrophages to promote lung fibrosis.[12] We here reported that N protein, encoded by wild-type or different variants of SARS-CoV-2 (such as Alpha, Beta, Gamma, Delta, and Omicron), could directly activate fibroblasts to induce pulmonary fibrosis. In pulmonary

---

(A and B) Determination of Smad3 localization in cells (scale bar, 10 μm) (A; the percentage of cells with Smand2/3 in the nucleus) and fractionation analysis (B; *, Smad2; **, Smad3).

(C) Top: N protein was transfected into control (Ctrl) or Smad3 knockdown (Smad3 KD) cells, and then the transcription activity was detected. Bottom: RMY-205 inhibited the N protein-induced transactivation activity of Smad dependent on Smad3[K41A]. Smad3 was first knocked down and then re-expression of Smad3 or Smad3[K41A] in 293T cells.

(D and F) Detection of mRNA levels of chemokines and cytokines (D) and recruitment of THP-1 macrophages and differential HL60 cells (scale bar, 100 μm) (F) with RMY-205 treatment.

(E) Recruitments of Smad2/3 to the promoters of cytokines with RMY-205 treatment.

The intensities of Western Blot bands relative to the loading control (such as Tubulin) were quantified and shown under each band. Statistical data are presented as the mean ± SEM. The differences between multiple groups were analyzed by using one-way or two-way ANOVA. *p < 0.05; **p < 0.01; ***p < 0.001; ns, not significant.
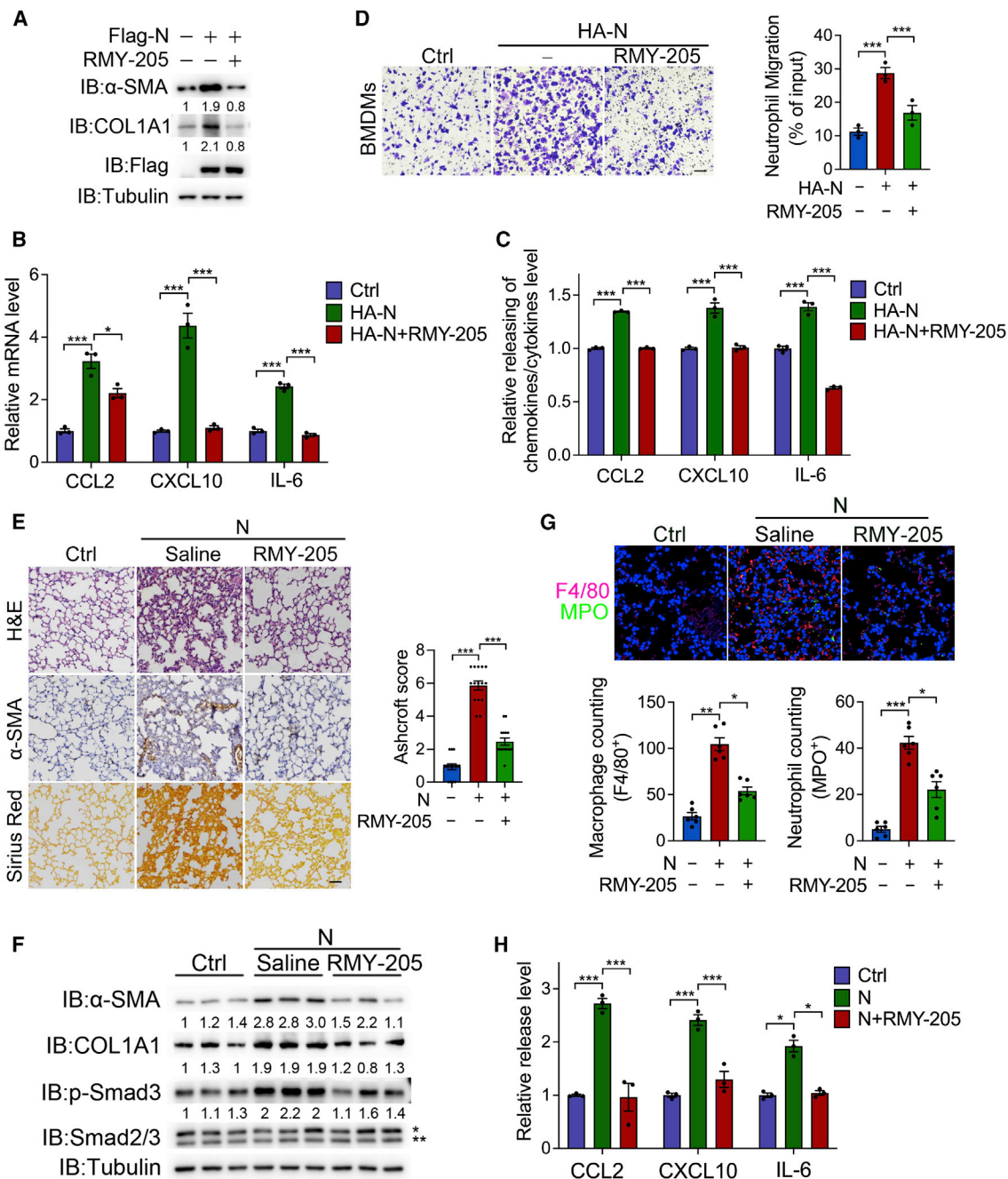
Figure 6. Physiological function of compound RMY-205 in the N protein-infected mouse model

Primary mouse pulmonary fibroblasts were isolated from the lungs of mice and then treated with RMY-205 (20 μM) for 36 h.

(A–D) The expression levels of α-SMA and COL1A1 (A), mRNA expression levels (B) and secretion levels (C) of cytokines and chemokines, and recruitment of primary bone marrow-derived macrophages (BMDMs) (scale bar, 10 μm) (D, left) and primary neutrophils (D, right).

(E–H) In the N protein-induced pulmonary fibrosis mouse model (n = 6 independent mice), expression of α-SMA and collagen deposition (scale bar, 100 μm) (E, left), and Ashcroft score (E, right) were evaluated in lung sections from RMY-205-treated mice. The infiltration of macrophages and neutrophils (G, top) was quantified (G, bottom). The content of cytokines in bronchoalveolar lavage fluid (BALF) from mice was detected (H). In the same samples, total cell lysates were prepared, and western blots were performed (F; *, Smad2; **, Smad3).

The intensities of Western Blot bands relative to the loading control (such as Tubulin) were quantified and shown under each band. Statistical data are presented as the mean ± SEM. The differences between multiple groups were analyzed by using one-way ANOVA. *p < 0.05; **p < 0.01; ***p < 0.001; ns, not significant.

Table 1. PK data for RMY-205 in ICR mice

Administration	$T_{1/2}$ (h)	AUC (0–∞) (ng/h/ mL)	T_{max} (h)	C_{max} (ng/mL)	CL (mL/min/kg)	Vss (mL/kg)	F (%)
I.v. (2 mg/kg)	1.98	995	–	–	34	3	–
I.p. (10 mg/kg)	8.26	2129	0.19	1,820	–	–	42.8
P.o. (10 mg/kg)	2.55	1871	0.33	1,039	–	–	37.6

I.v., intravenous; p.o., per os; $T_{1/2}$, half-life; AUC, area under the curve; CL, clearance; Vss, steady-state apparent distribution volume; C_{max}, maximal concentration; T_{max}, time of maximal concentration in hours; F, bioavailability.

fibroblasts, binding of N protein with TβRI competitively disrupted the interaction between TβRI and FKBP12, leading to polymerization and phosphorylation of TβRI in a TβRII-independent manner. TβRI consequently phosphorylated Smad2/3 to promote their transactivation activity, which not only induced the expression of pro-fibrotic genes, such as COL1A1 and α-SMA, but also facilitated the expression and secretion of cytokines (IL-6, IL-8, CCL2, and CXCL10) for recruitment of macrophages and neutrophils to jointly promote pulmonary fibrosis. We further discovered a compound, RMY-205, that directly targeted Smad3 and blocked activation of Smad3 by TβRI, thereby alleviating pulmonary fibrosis (Figure 7). The SAR analysis suggested that the compounds would have stronger interaction with Smad3 than with α-SMA, with an H group at the R_1 position, a 2,4 double substitution, as well as a para-substitution of Br at the benzene ring.

TGF-β signaling is the most intensively studied pathway involved in regulation of fibrosis, and production of TGF-β has been linked to development of fibrosis in several diseases, including pulmonary fibrosis.[32] Recently, it was reported that SARS-CoV-2-encoded N protein could bind to Smad3 to elevate Smad3 activity with TGF-β stimulation in renal tubular epithelial cells, leading to tubular epithelial cell death and acute kidney injury.[33] However, the interaction of N protein with Smad3 was not detected in pulmonary fibroblasts in our study, suggesting that the regulatory function of the viral protein is cell type and context dependent. Instead, we found that N protein interacted with TβRI to activate the TβRI-Smad3 pathway in the absence of TGF-β. In canonical TGF-β signaling, TGF-β binds to TβRII to initiate formation of a heterotetrameric complex with two TβRI and two TβRII molecules,[34–36] leading to phosphorylation of TβRI in the GS domain (SGSGSG motif) by the constitutively activated TβRII.[37] This phosphorylation induces a conformational change of TβRI that causes the release of FKBP12,[36,38,39] thereby activating TβRI to phosphorylate Smad2/3. Thus, FKBP12 functions as a gatekeeper for TGF-β signaling by preventing inadvertent activation of TβRI in the absence of a ligand. The current study demonstrated that expression of N protein led to competitive release of FKBP12 from TβRI, thus liberating the TβRI kinase to bypass the signal initiated from TGF-β to TβRII. In this regard, parallel to the extracellular ligand-initiated TβRI activation, the SARS-CoV-2-encoded N protein could function as an intracellular TβRI activator that hijacks the TβRI-Smad3 signaling for progression of pulmonary fibrosis in a TGF-β- or TβRII-independent manner. Although we have demonstrated that N protein-induced activation of TGF-β signaling promotes pulmonary fibrosis not only in pulmonary fibroblasts but also in mice that were infected with an AAV encoding N protein, it is worthwhile to further investigate whether it is the N protein, but not other SARS-CoV-2-encoded proteins, that activates TGF-β signaling

in the SARS-CoV-2-infected mouse model. Moreover, the function of RMY-205 in the SARS-CoV-2-infected mouse model also deserved further investigation.

It is generally considered that fibrosis is the result of excessive wound repair, which is caused by chronic inflammation.[40] Here, we demonstrated that N protein-induced activation of pulmonary fibroblasts also facilitated establishment of an inflammatory environment. Activation of Smad3 by N protein not only facilitated expression of pro-fibrotic proteins but also stimulated secretion of cytokines, including IL-6, IL-8, CCL2, and CXCL10. On one hand, CCL2 and CXCL10 facilitate recruitment of inflammatory cells, such as macrophages and neutrophils, which might further exacerbate inflammation and partially contribute to the "cytokine storm" in COVID-19 patients. On the other hand, IL-6, IL-8, as well as macrophages/neutrophils also take part in the progression of pulmonary fibrosis,[12,32] thus forming a feedforward loop to further aggravate pulmonary fibrosis. This may at least partially explain why many severe COVID-19 patients develop serious pulmonary fibrosis, which results in chronic respiratory failure.[1] Therefore, targeting N protein-activated TβRI-Smad3 signaling may represent as a promising strategy for ameliorating SARS-CoV-2-induced lung lesions.

Compound RMY-205, screening from our in-house library, was shown to effectively inhibit pulmonary fibrosis in the current case. Although RMY-205 did not influence the interaction of N protein with TβRI, it bound to Smad3 to disrupt the interaction of TβRI with Smad3, thus impeding activation of TβRI-Smad3 signaling. Interestingly, RMY-205 bound to the Smad3 MH1 domain, which is responsible for DNA binding,[36] but its function was to enhance the association with the MH2 domain to hinder interaction with TβRI. Based on the model of molecular docking, RMY-205 might function as "molecular glue" to promote the intramolecular interaction between the MH1 and MH2 domains of Smad3, which results in steric hindrance to block TβRI binding to the MH2 domain. Given the important role of the MH1 domain in DNA binding, the RMY-205-induced closed conformation might also block Smad3's DNA binding activity to attenuate its transactivation activity. Therefore, it appears that RMY-205 may suppress TβRI-Smad3 signaling through a multipronged mechanism.

TβRI is required to activate the canonical TGF-β-Smad signaling pathway as well as non-canonical pathways, including the mitogen-associated protein kinase (MAPK), phosphatidylinositol 3-kinase (PI3K)-Akt, and nuclear factor κB (NF-κB) pathways,[36] which may lead to more activation events through various TβRI-associated targets. In contrast to Smad3 deficiency, TβRI deficiency is lethal in mice,[41,42] suggesting that Smad3 might be a better therapeutic target than TβRI[11,43] and that targeting Smad3 instead of TβRI might achieve an effective anti-fibrotic function with fewer side effect. In our case, during
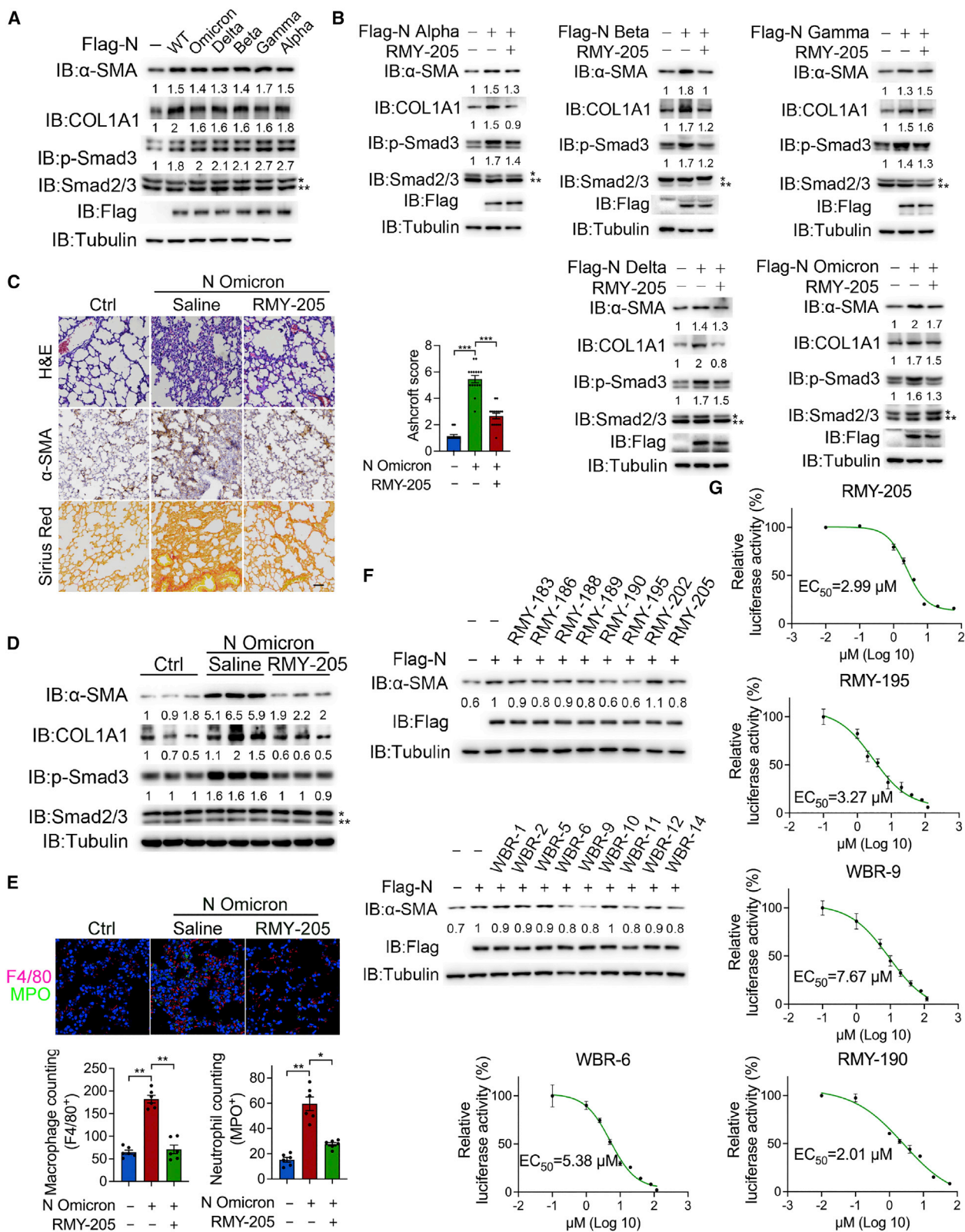
Figure 7. Effects of compound RMY-205 on pulmonary fibrosis induced by different N protein variants

(A) Primary mouse pulmonary fibroblasts were isolated from mice, N protein from different SARS-CoV-2 variants was transfected into cells, and the expression levels of α-SMA, COL1A1, and Smad3 phosphorylation were determined (*, Smad2; **, Smad3).

administration of RMY-205, mice showed no abnormal behavior or weight loss of the body or various organs, while RMY-205 showed a markedly anti-fibrotic effect in the mouse model of N protein-induced pulmonary fibrosis. Recently, Qiao et al.[44] identified six compounds suitable for *in vivo* viral inhibition of SARS-CoV-2, among which two compounds had fairly good PK properties with oral bioavailability of 11.2% and 14.6%, respectively. The PK properties of RMY-205 also had favorable characteristics, and the oral bioavailability of 37.6% indicated that RMY-205 was of great potential to be an oral drug candidate for SARS-CoV-2-induced pulmonary fibrosis because a compound with oral bioavailability of greater than 10% would be of great value for development as an oral drug.[45]

In addition to pulmonary fibrosis induced by N protein of SARS-CoV-2 and its variants, RMY-205 has much broader functions in inhibiting tissue fibrosis. RMY-205 is an effective inhibitor of TGF-β/Smad signaling by binding to Smad3 but not N protein, and this inhibitory effect could be observed in different cell lines and different mouse models. Because TGF-β/Smad signaling is the master pathway that regulates tissue fibrosis, it is not surprising that RMY-205 could broadly suppress TGF-β/Smad signaling-associated fibrosis in different tissues. Future efforts will be invested in structure-based optimization of RMY-205 to develop the compound into a drug candidate for treating SARS-CoV-2-induced pulmonary fibrosis.

Limitations of the study

It is well known that pulmonary fibrosis is a typical sequela of COVID-19, and activation of TGF-β signaling is widely recognized in lung fibroblasts. In this study, we demonstrated that N protein-induced activation of TGF-β signaling promotes pulmonary fibrosis not only in pulmonary fibroblasts but also in mice that were infected with an AAV encoding N protein. However, it is worthwhile to investigate (1) whether it is the N protein, but not other SARS-CoV-2-encoded proteins, that activates TGF-β signaling in the SARS-CoV-2-infected mouse model and (2) whether the interaction of the N protein with the TGF-β receptor can be observed in SARS-CoV-2-infected tissue and whether this constitutively activates the Smad pathway. Moreover, the function of RMY-205 in the SARS-CoV-2-infected mouse model also deserves further investigation.

SIGNIFICANCE

Pulmonary fibrosis is a typical sequela of coronavirus disease 2019 (COVID-19) with poor prognosis for COVID-19 patients. However, whether there is a direct connection between virus infection and pulmonary fibrosis and how virus infection changes the lung environment is still unclear in COVID-19 patients. SARS-CoV-2 has a genome of approximately 30,000 nt, encoding various structural, non-structural, and accessory proteins. Among the four structural proteins, N protein is most abundant. In this study, we found that the N protein-activated TGF-β signaling pathway is responsible for the occurrence of pulmonary fibrosis. N protein binds to the TGF-β receptor TβRI to competitively disrupt the interaction of TβRI with its upstream factor FKBP12, which leads to formation of TβRI polymers and consequently activates TβRI. Activated TβRI induces downstream transcription factor Smad3 translocation from the cytosol to the nucleus, where Smad3 promotes expression of pro-fibrotic genes and secretion of cytokines, leading to recruitment of macrophages and neutrophils, resulting in progression of pulmonary fibrosis. Furthermore, a compound named RMY-205 (2-(4-(4-bromo-2-fluorobenzyl) piperazin-1-yl)-3-hydroxy-4H-chromen-4-one) was identified from the in-house compound library with an ability to relieve SARS-CoV-2-induced pulmonary fibrosis. RMY-205 directly binds to Smad3 to interdict N protein-induced Smad3-TβRI interaction, which attenuates Smad3-activated downstream target genes and inhibits the release of cytokines. RMY-205 is also effective for inhibiting pulmonary fibrosis induced by N protein from different SARS-CoV-2 variants, including Alpha, Beta, Gamma, Delta, and Omicron. In an N protein-induced mouse pulmonary fibrosis model, after p.o. administration, RMY-205 showed a $T_{1/2}$ of 2.55 h, bioavailability of 37.6%, and clearance (CL) rate of 34 mL/min/kg, demonstrating the potential of RMY-205 as an oral drug. This study highlights a signaling pathway of pulmonary fibrosis induced by N protein and demonstrates a novel therapeutic strategy for pulmonary fibrosis by compound RMY-205 targeting of Smad3.

STAR★METHODS

Detailed methods are provided in the online version of this paper and include the following:

- KEY RESOURCES TABLE
- RESOURCE AVAILABILITY
  - Lead contact
  - Materials availability
  - Data and code availability
- EXPERIMENTAL MODEL AND SUBJECT DETAILS
  - Animals
  - AAV administration mouse model
  - Adriamycin nephropathy mouse model
  - Cell lines and cell culture

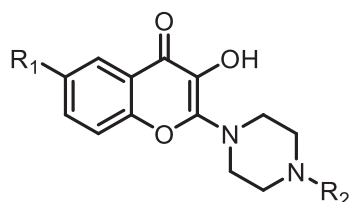(B) Cells as in (A) were treated with RMY-205 (20 μM) for 36 h, and western blots were performed.

(C–E) In the mouse model of pulmonary fibrosis induced by the N protein of the Omicron variant (n = 6 independent mice), expression of α-SMA and collagen deposition (scale bar, 100 μm) (C, left) and Ashcroft score (C, right) were evaluated in lung sections from RMY-205-treated mice. The infiltration of macrophages and neutrophils (E, top) was quantified (E, bottom). In the same samples, western blots were performed (D).
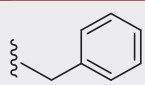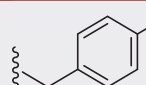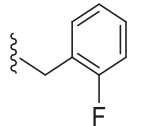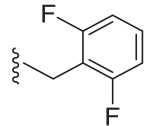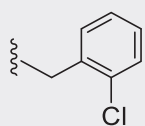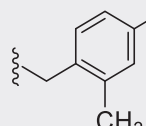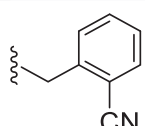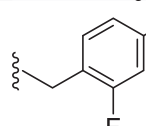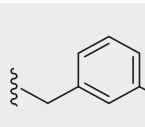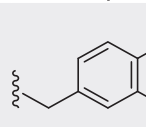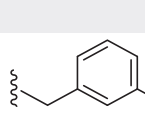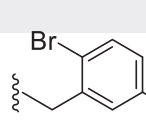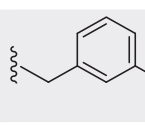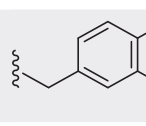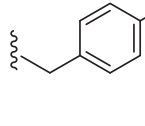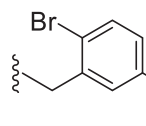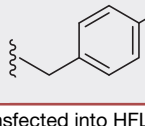
(F) The SAR analysis of RMY-205. N-protein was transfected into HFL-1 cells and then treated with different RMY-205 derivatives (10 μM) for 36 h. The expression levels of α-SMA were determined.

(G) N protein was transfected into HFL-1 cells, and the transcription activity was detected at different concentrations of RMY-205.

The intensities of Western Blot bands relative to the loading control (such as Tubulin) were quantified and shown under each band. Statistical data are presented as the mean ± SEM. The differences between multiple groups were analyzed by using one-way ANOVA. *p < 0.05; **p < 0.01; ***p < 0.001; ns, not significant.

Table 2. SAR analysis of RMY-205 in α-SMA inhibition

Compound	R₁	R₂	α-SMA inhibition ratio (%)	Compound	R₁	R₂	α-SMA inhibition ratio (%)
RMY-189	H	(benzyl)	24.8 ± 13.2	RMY-190	H	(4-Br-benzyl)	105.4 ± 18.3
RMY-188	H	(2-F-benzyl)	7.3 ± 8.8	WBR-9	H	(2,6-diF-benzyl)	40.4 ± 7.8
RMY-183	H	(2-Cl-benzyl)	25.1 ± 5.7	RMY-195	H	(4-F-2-CH₃-benzyl)	96.2 ± 8.8
WBR-14	H	(2-CN-benzyl)	17.5 ± 11.5	RMY-205	H	(4-Br-2-F-benzyl)	50.9 ± 14.0
WBR-10	H	(3-F-benzyl)	−4 ± 1.2	WBR-1	F	(3,4-diCl-benzyl)	29.5 ± 13.4
WBR-12	H	(3-Cl-benzyl)	20.3 ± 8.0	WBR-2	F	(2-Br-4-OCH₃-benzyl)	25.1 ± 1.6
RMY-186	H	(3-Br-benzyl)	23.2 ± 9.9	WBR-5	Br	(3,4-diCl-benzyl)	24.8 ± 6.6
WBR-11	H	(4-F-benzyl)	26.8 ± 9.0	WBR-6	Br	(2-Br-4-OCH₃-benzyl)	32.8 ± 19.8
RMY-202	H	(4-Cl-benzyl)	−9.4 ± 13.4				

N-protein was transfected into HFL-1 cells and then treated with different RMY-205 derivatives (10 μM) as indicated for 24 h.

- ● METHOD DETAILS
  - ○ Plasmid constructions
  - ○ Generation of the lentiviral system
  - ○ Immunoprecipitation and western blotting
  - ○ Quantitative reverse transcription PCR
  - ○ Chromatin immunoprecipitation (ChIP) assay
  - ○ GST pull-down assay
  - ○ Immunohistochemistry and scoring
  - ○ Immunofluorescence
  - ○ Transwell chemotaxis assay
  - ○ Analysis of cytokines production
  - ○ Collagen detection

- ○ ITC assay
- ○ Luciferase assay
- ○ Construction of recombinant adeno-associated virus
- ○ ELISA assay
- ○ Isolation of mouse primary pulmonary fibroblasts, BMDMs and neutrophils
- ○ Crosslinking assay
- ○ Subcellular fractionation
- ○ The SAR analysis of RMY-205 derivatives
- ○ Determination of EC_{50}
- ○ Detection of RMY-205 pharmacokinetic (PK) properties
- ○ The synthesis of compound RMY-205
- ○ NMR ans MS data for RMY-205 derivatives
- ● QUANTIFICATION AND STATISTICAL ANALYSIS

AUTHOR CONTRIBUTIONS

Q.W., F.-N.L., and T.L. conceived this study, proposed the hypotheses, designed the experiments, and wrote, reviewed, and edited the manuscript. Q.W.'s group, including Z.-y.Z., C.-y.J., L.-z.W., H.-Z.C., P.-b.Y., X.-y.C., Z.-h.J., and W.-j.W. performed biological and mouse experiments and analyzed data. F.-n.L.'s group, including H.Y., B.-R.W., and T.G., designed and synthesized the compounds. T.L.'s group, including W.-b.H., analyzed the docking model of RMY-205 binding to Smad, expressed the individual domains of MH1 and MH2 of Smad3 in *E. coli*, and assisted with the ITC experiment.

DECLARATION OF INTERESTS

The authors declare no competing interests.

INCLUSION AND DIVERSITY

We support inclusive, diverse, and equitable conduct of research.

REFERENCES

1. Lamers, M.M., and Haagmans, B.L. (2022). SARS-CoV-2 pathogenesis. Nat. Rev. Microbiol. *20*, 270–284.

2. Wang, C., Horby, P.W., Hayden, F.G., and Gao, G.F. (2020). A novel coronavirus outbreak of global health concern. Lancet *395*, 470–473.

3. Nalbandian, A., Sehgal, K., Gupta, A., Madhavan, M.V., McGroder, C., Stevens, J.S., Cook, J.R., Nordvig, A.S., Shalev, D., Sehrawat, T.S., et al. (2021). Post-acute COVID-19 syndrome. Nat. Med. *27*, 601–615.

4. George, P.M., Wells, A.U., and Jenkins, R.G. (2020). Pulmonary fibrosis and COVID-19: the potential role for antifibrotic therapy. Lancet Respir. Med. *8*, 807–815.

5. John, A.E., Joseph, C., Jenkins, G., and Tatler, A.L. (2021). COVID-19 and pulmonary fibrosis: a potential role for lung epithelial cells and fibroblasts. Immunol. Rev. *302*, 228–240.

6. Wu, X., Liu, X., Zhou, Y., Yu, H., Li, R., Zhan, Q., Ni, F., Fang, S., Lu, Y., Ding, X., et al. (2021). 3-month, 6-month, 9-month, and 12-month respiratory outcomes in patients following COVID-19-related hospitalisation: a prospective study. Lancet Respir. Med. *9*, 747–754.

7. Bai, C., Zhong, Q., and Gao, G.F. (2022). Overview of SARS-CoV-2 genome-encoded proteins. Sci. China Life Sci. *65*, 280–294. https://doi.org/10.1007/s11427-021-1964-4.

8. Carlson, C.R., Asfaha, J.B., Ghent, C.M., Howard, C.J., Hartooni, N., Safari, M., Frankel, A.D., and Morgan, D.O. (2020). Phosphoregulation of phase separation by the SARS-CoV-2 N protein suggests a biophysical basis for its dual functions. Mol. Cell *80*, 1092–1103.e4.

9. Yang, H., and Rao, Z. (2021). Structural biology of SARS-CoV-2 and implications for therapeutic development. Nat. Rev. Microbiol. *19*, 685–700.

10. Wang, S., Dai, T., Qin, Z., Pan, T., Chu, F., Lou, L., Zhang, L., Yang, B., Huang, H., Lu, H., and Zhou, F. (2021). Targeting liquid–liquid phase separation of SARS-CoV-2 nucleocapsid protein promotes innate antiviral immunity by elevating MAVS activity. Nat. Cell Biol. *23*, 718–732.

11. Meng, X.M., Nikolic-Paterson, D.J., and Lan, H.Y. (2016). TGF-β: the master regulator of fibrosis. Nat. Rev. Nephrol. *12*, 325–338.

12. Wendisch, D., Dietrich, O., Mari, T., von Stillfried, S., Ibarra, I.L., Mittermaier, M., Mache, C., Chua, R.L., Knoll, R., Timm, S., et al. (2021). SARS-CoV-2 infection triggers profibrotic macrophage responses and lung fibrosis. Cell *184*, 6243–6261.e27.

13. Delorey, T.M., Ziegler, C.G.K., Heimberg, G., Normand, R., Yang, Y., Segerstolpe, Å., Abbondanza, D., Fleming, S.J., Subramanian, A., Montoro, D.T., et al. (2021). COVID-19 tissue atlases reveal SARS-CoV-2 pathology and cellular targets. Nature *595*, 107–113.

14. Hinz, B., Celetta, G., Tomasek, J.J., Gabbiani, G., and Chaponnier, C. (2001). Alpha-smooth muscle actin expression upregulates fibroblast contractile activity. Mol. Biol. Cell *12*, 2730–2741.

15. Wilson, M.S., and Wynn, T.A. (2009). Pulmonary fibrosis: pathogenesis, etiology and regulation. Mucosal Immunol. *2*, 103–121.

16. Sime, P.J., Xing, Z., Graham, F.L., Csaky, K.G., and Gauldie, J. (1997). Adenovector-mediated gene transfer of active transforming growth factor-beta1 induces prolonged severe fibrosis in rat lung. J. Clin. Invest. *100*, 768–776.

17. Ashcroft, T., Simpson, J.M., and Timbrell, V. (1988). Simple method of estimating severity of pulmonary fibrosis on a numerical scale. J. Clin. Pathol. *41*, 467–470.

18. Souchelnytskyi, S., ten Dijke, P., Miyazono, K., and Heldin, C.H. (1996). Phosphorylation of Ser165 in TGF-beta type I receptor modulates TGF-beta1-induced cellular responses. EMBO J. *15*, 6231–6240.

19. Chen, Y.-G., Liu, F., and Massague, J. (1997). Mechanism of TGFβ receptor inhibition by FKBP12. EMBO J. *16*, 3866–3876.

20. Wojciech, S., Ahmad, R., Belaid-Choucair, Z., Journé, A.S., Gallet, S., Dam, J., Daulat, A., Ndiaye-Lobry, D., Lahuna, O., Karamitri, A., et al. (2018). The orphan GPR50 receptor promotes constitutive TGFβ receptor signaling and protects against cancer development. Nat. Commun. *9* (1), 1216.

21. Derynck, R., and Zhang, Y.E. (2003). Smad-dependent and Smad-independent pathways in TGF-b family signalling. Nature *425*, 577–584.

22. Dijke, P.t., and Hill, C.S. (2004). New insights into TGF-β–Smad signalling. Trends Biochem. Sci. *29*, 265–273.

23. Jinnin, M., Ihn, H., and Tamaki, K. (2006). Characterization of SIS3, a novel specific inhibitor of Smad3, and its effect on transforming growth factor-β1-induced extracellular matrix expression. Mol. Pharmacol. *69*, 597–607.

24. Zhu, S., Wang, W., Clarke, D.C., and Liu, X. (2007). Activation of Mps1 promotes transforming growth factor-β-independent Smad signaling. J. Biol. Chem. *282*, 18327–18338.

25. Nakao, A., Imamura, T., Souchelnytskyi, S., Kawabata, M., Ishisaki, A., Oeda, E., Tamaki, K., Hanai, J., Heldin, C.H., Miyazono, K., and ten Dijke, P. (1997). TGF-β receptor-mediated signalling through Smad2, Smad3 and Smad4. EMBO J. *16*, 5353–5362.

26. Wynn, T.A., Chawla, A., and Pollard, J.W. (2013). Macrophage biology in development, homeostasis and disease. Nature *496*, 445–455.

27. Mantovani, A., Cassatella, M.A., Costantini, C., and Jaillon, S. (2011). Neutrophils in the activation and regulation of innate and adaptive immunity. Nat. Rev. Immunol. *11*, 519–531.

28. Del Valle, D.M., Kim-Schulze, S., Huang, H.H., Beckmann, N.D., Nirenberg, S., Wang, B., Lavin, Y., Swartz, T.H., Madduri, D., Stock, A., et al. (2020). An inflammatory cytokine signature predicts COVID-19 severity and survival. Nat. Med. *26*, 1636–1643.

29. Tamaki, K., Okuda, S., Ando, T., Iwamoto, T., Nakayama, M., and Fujishima, M. (1994). TGF-β1 in glomerulosclerosis and interstitial fibrosis of adriamycin nephropathy. Kidney Int. *45*, 525–536.

30. Andrews, N., Stowe, J., Kirsebom, F., Toffa, S., Rickeard, T., Gallagher, E., Gower, C., Kall, M., Groves, N., O'Connell, A.M., et al. (2022). Covid-19 vaccine effectiveness against the omicron (B.1.1.529) variant. N. Engl. J. Med. *386*, 1532–1546.

31. Michalski, J.E., Kurche, J.S., and Schwartz, D.A. (2022). From ARDS to pulmonary fibrosis: the next phase of the COVID-19 pandemic? Transl. Res. *241*, 13–24.

32. Heukels, P., Moor, C.C., von der Thüsen, J.H., Wijsenbeek, M.S., and Kool, M. (2019). Inflammation and immunity in IPF pathogenesis and treatment. Respir. Med. *147*, 79–91.

33. Wang, W., Chen, J., Hu, D., Pan, P., Liang, L., Wu, W., Tang, Y., Huang, X.R., Yu, X., Wu, J., and Lan, H.Y. (2022). SARS-CoV-2 N protein induces acute kidney injury via smad3-dependent G1 cell cycle arrest mechanism. Adv. Sci. *9*, 2103248.

34. Hinck, A.P., Mueller, T.D., and Springer, T.A. (2016). Structural biology and evolution of the TGF-β family. Cold Spring Harbor Perspect. Biol. *8*, a022103.

35. Ehrlich, M., Gutman, O., Knaus, P., and Henis, Y.I. (2012). Oligomeric interactions of TGF-β and BMP receptors. FEBS Lett. *586*, 1885–1896.

36. Deryneck, R., and Budi, E.H. (2019). Specificity, versatility, and control of TGF-β family signaling. Sci. Signal. *12*, eaav5183.

37. Wrighton, K.H., Lin, X., and Feng, X.-H. (2009). Phospho-control of TGF-β superfamily signaling. Cell Res. *19*, 8–20.

38. Huse, M., Chen, Y.-G., Massagué, J., and Kuriyan, J. (1999). Crystal structure of the cytoplasmic domain of the type I TGF^N_L receptor in complex with FKBP12. cell *96*, 425–436.

39. Huse, M., Muir, T.W., Xu, L., Chen, Y.G., Kuriyan, J., and Massagué, J. (2001). The TGF^N_L receptor activation process: an inhibitor- to substrate-binding switch. Mol. Cell *8*, 671–682.

40. Wynn, T.A. (2011). Integrating mechanisms of pulmonary fibrosis. J. Exp. Med. *208*, 1339–1350.

41. Goumans, M.-J., and Mummery, C. (2000). Functional analysis of the TGFβ receptor/Smad pathway through gene ablation in mice. Int. J. Dev. Biol. *44*, 253–265.

42. Seki, T., Hong, K.-H., and Oh, S.P. (2006). Nonoverlapping expression patterns of ALK1 and ALK5 reveal distinct roles of each receptor in vascular development. Lab. Invest. *86*, 116–129.

43. Deryneck, R., Turley, S.J., and Akhurst, R.J. (2021). TGFβ biology in cancer progression and immunotherapy. Nat. Rev. Clin. Oncol. *18*, 9–34.

44. Qiao, J., Li, Y.S., Zeng, R., Liu, F.L., Luo, R.H., Huang, C., Wang, Y.F., Zhang, J., Quan, B., Shen, C., et al. (2021). SARS-CoV-2 M[pro] inhibitors with antiviral activity in a transgenic mouse model. Science *371*, 1374–1378.

45. Martin, Y.C. (2005). A bioavailability score. J. Med. Chem. *48*, 3164–3170.

46. Wang, W.j., Wang, Y., Chen, H.z., Xing, Y.z., Li, F.w., Zhang, Q., Zhou, B., Zhang, H.k., Zhang, J., Bian, X.l., et al. (2014). Orphan nuclear receptor TR3 acts in autophagic cell death via mitochondrial signaling pathway. Nat. Chem. Biol. *10*, 133–140.

47. Hou, P.P., Luo, L.J., Chen, H.Z., Chen, Q.T., Bian, X.L., Wu, S.F., Zhou, J.X., Zhao, W.X., Liu, J.M., Wang, X.M., et al. (2020). Ectosomal PKM2 promotes HCC by inducing macrophage differentiation and remodeling the tumor microenvironment. Mol. Cell *78*, 1192–1206.e10.

48. Riches, D.W.H., and Martin, T.R. (2018). Overview of innate lung immunity and inflammation. Methods Mol. Biol. *1809*, 17–30.

49. Bian, X.L., Chen, H.Z., Yang, P.B., Li, Y.P., Zhang, F.N., Zhang, J.Y., Wang, W.J., Zhao, W.X., Zhang, S., Chen, Q.T., et al. (2017). Nur77 suppresses hepatocellular carcinoma via switching glucose metabolism toward gluconeogenesis through attenuating phosphoenolpyruvate carboxykinase sumoylation. Nat. Commun. *8*, 14420.

STAR★METHODS

KEY RESOURCES TABLE

REAGENT or RESOURCE	SOURCE	IDENTIFIER
Antibodies		
The goat anti-rabbit antibody	Thermo Fisher	Cat#31210; RRID: AB_228341
The goat anti-mouse antibody	Thermo Fisher	Cat#31160; RRID: AB_228297
Mouse monoclonal anti-β-Tubulin for WB	Sigma-Aldrich	Cat#T4026; RRID: AB_477577
Mouse monoclonal anti-Flag for WB and IP	Sigma-Aldrich	Cat#F3165; RRID: AB_2572291
Mouse monoclonal anti-HA for WB and IP	Sigma-Aldrich	Cat#H9658; RRID: AB_390918
VeriBlot reagents for IP detection	Abcam	Cat#ab131366; RRID: AB_2892718
Rabbit monoclonal anti-α-SMA for WB and IF	Abcam	Cat#ab124964; RRID: AB_11129103
Rat monoclonal anti-F4/80 for IF	Abcam	Cat#ab6640; RRID: AB_1140040
Rabbit Polyclonal Anti-p-TGFBR1 (T204) for WB	Affinity Biosciences	Cat#AF8456; RRID: AB_2840510
Rabbit Polyclonal Anti-Smad2/3 for WB and IF	Servicebio	Cat#GB111844
Rabbit Polyclonal Anti-MPO for IF	Servicebio	Cat#GB11224; RRID: AB_2814688
Rabbit Polyclonal Anti-TGFBR1 for WB	ABclonal	Cat#A0708; RRID: AB_2757355
Rabbit Polyclonal Anti-FKBP12 for WB	ABclonal	Cat#A17638; RRID: AB_2763806
Rabbit Polyclonal Anti-p-Smad3 S423/425 for WB and IF	ABclonal	Cat#AP0727; RRID: AB_2863813
Rabbit Polyclonal Anti-p-Smad2 S465/467 for WB	ABclonal	Cat#AP0925; RRID: AB_2863837
Rabbit Polyclonal Anti-TGFBR2 for WB	Proteintech	Cat# 27212-1-AP; RRID: AB_2918119
Mouse monoclonal anti-IL-6 for neutralization	Proteintech	Cat# 69001-1-Ig; RRID: AB_2918847
Goat Polyclonal anti IL-8 for neutralization	R&D Systems	Cat# AF-208-SP; RRID: AB_354394
Rat monoclonal anti-HA for WB and IF	Roche	Cat#11867423001;RRID: AB_390918
Rabbit monoclonal anti-Flag for WB and IF	Cell Signaling Technology	Cat#14793; RRID: AB_2572291
Bacterial strains		
E.coli DH5α	TIANGEN Biotech	Cat#CB101
E.coli BL21	TIANGEN Biotech	Cat#CB105
Chemicals, peptides, and recombinant proteins		
Sirius red	Servicebio	Cat#G1018
Diamidino-2-phenylindole (DAPI)	Thermo Fisher Scientific	Cat#62247
TGF-β	Cell Signaling Technology	Cat#8915LC
Human IL-6	Sino Biological	Cat#10395-HNAE
Human CCL2	Sino Biological	Cat# 10134-H08Y
Human IL-8	MCE	Cat#HY-P9379
Human CXCL10	MCE	Cat# HY-P7226
GoTaq qPCR Master Mix	Promega	Cat#A6001
Optiprep	Sigma-Aldrich	Cat#D1556
Critical commercial assays		
Human Inflammation Array C3	Raybiotech	AAH-INF-3
Mouse CXCL10/IP10 ELISA Kit	ABclonal	RK00056
Mouse IL-6 ELISA Kit	ABclonal	RK00008
Mouse CCL2 ELISA Kit	ABclonal	RK00381
Mouse CXCL15 ELISA Kit	Biosharp	BSEM-076-96T

(Continued on next page)

Continued

REAGENT or RESOURCE	SOURCE	IDENTIFIER
UltraSensitive SP IHC Kit	MXB	Kit-9730
Deposited data		
CCL2	ChIP-atlas	SRX148895
IL-6	ChIP-atlas	SRX5757568
IL-8	ChIP-atlas	SRX5757564
CXCL10	ChIPBase	GSM1266817
Experimental models: Cell lines		
HEK293T	Cell Bank of Chinese Academy of Sciences	GNHu17
THP-1	IMMOCELL	IM-H260
HFL-1	Dongyangguang Dr.Shengtian Cao	CCL-153
HL-60	XMU Dr.Xianming Deng	CCL-240
Experimental models: Organisms/strains		
C57BL/6J mice	Jackson Laboratory animal	N/A
Oligonucleotides		
Ctrl shRNA (pLKO.1) CAACAAGATGAAGAGCACCAA	This paper	N/A
h.CXCL10 shRNA (pLKO.1) GGAGTATATGTCAAGCCATAA	This paper	N/A
h.CCL2 shRNA (pLKO.1) GGACAAGCAAACCCAAACTCC	This paper	N/A
h.CXCL10 shRNA (pLKO.1) GGAGTATATGTCAAGCCATAA	This paper	N/A
h.TGFBR2 shRNA (pLKO.1) GCTCCAGAAGTCCTAGAATCC	This paper	N/A
h.FKBP12 shRNA (pLKO.1) GGACAGAAACAAGCCCTTTAA	This paper	N/A
h.TGFBR1 shRNA (pLKO.1) GCTTAGTATTCTGGGAAATTG	This paper	N/A
h.Smad3 shRNA (pLKO.1) GGTGACAACTATAGCAGTT	This paper	N/A
h.Smad2 shRNA (pLKO.1) GCTGTAATCTGAAGATCTT	This paper	N/A
Softwares and algorithms		
ImageJ	open source	https://imagej.net
GraphPad 8	open source	https://www.graphpad.com/

RESOURCE AVAILABILITY

Lead contact

Further information and requests for resources and reagents should be directed to and will be fulfilled by the lead contact, Qiao wu (qiaow@xmu.edu.cn).

Materials availability

Plasmids and cell lines generated in this study are available by request to the lead contact. RMY-205 and its derivates generated in this study will be made available on request, but we may require a payment and/or a completed Materials Transfer Agreement if there is potential for commercial application.

Data and code availability

This paper analyzes existing, publicly available data. These accession numbers for the datasets are listed in the key resources table.

This paper does not report original code.

Any additional information required to reanalyze the data reported in this paper is available from the lead contact upon request.

EXPERIMENTAL MODEL AND SUBJECT DETAILS

Animals

All mice were maintained on 12 h light/12 h dark cycle with free access to food and water and housed under specific pathogen-free (SPF) conditions at the Xiamen University Laboratory Animal Center. All of the animal experiments were approved by the Animal Ethics Committee of Xiamen University (Acceptance No. XMULAC20190048).

AAV administration mouse model

For the AAV administration mouse model (Gauldie et al.,1997), 8-weeks-old male C57BL/6J mice were intranasally (IN) instilled with 1×10^9 titers of N AAV or control AAV resuspended in 50 μL PBS. Starting at day 4, the mice were intraperitoneally injected with RMY-205 (10 mg/kg in saline) weekly. The mice were sacrificed and examined after 30 days.

Adriamycin nephropathy mouse model

For the adriamycin nephropathy mouse model, 8-weeks-old male C57BL/6J mice were administrated with a single tail vein injection of Adriamycin (18 mg/kg in saline). Starting at day 1, the mice were intraperitoneally injected with RMY-205 (3 mg/kg in saline) daily. The mice were sacrificed and examined after 7 days.

Cell lines and cell culture

HFL-1 (orign: human, male, fetus, CCL-153); HEK293T (orign: human, female, fetus, GNHu17); THP-1 (orign: human, male, 1-year-old, IM-H260); HL-60 (orign: human, female, 36-years-old, CCL-153). HFL-1 cells were cultured in Ham's F-12 medium, mouse primary pulmonary fibroblasts, mouse primary BMDMs and HEK293T cells were cultured in Dulbecco's modified Eagle's medium, THP-1, HL-60 cells and mouse primary neutrophils were cultured in RPMI-1640 medium. All cell lines were supplemented with 10% FBS, penicillin (100 IU) and streptomycin (100 mg/mL) (Bio Basic Inc., Shanghai, China), and maintained at 37°C in an atmosphere containing 5% CO_2, tested negative for mycoplasma contamination. Transfections were carried out using the calcium-phosphate precipitation method for HEK293T cells with the ViaFect Transfection Reagent (Promega, Madison, WI, USA) for HFL-1 cells.

METHOD DETAILS

Plasmid constructions

The plasmids of SARS-CoV-2-encoded proteins were obtained from National Center for Protein Science (Shanghai, China), and then cloned into p3×Flag-CMV-10 or pCMV5-HA. N protein from original SARS-CoV-2 and other variants was cloned into p3×Flag-CMV-10, pCMV5-HA, plenti-EGFP or pAAV-EGFP. Human TβRI, TBR2, Smad3, Smad2, Smad3-MH1, and Smad3-MH2 was cloned into p3×Flag-CMV-10, pCMV5-HA, or plenti-EGFP.

Generation of the lentiviral system

The lentiviral-based vector pLKO.1 was used to express shRNA in cells. The oligonucleotides were annealed and subcloned into the lentiviral pLKO.1. The pLKO.1 shRNA and lentiviral packing plasmids were transfected into HEK293T cells to generate lentiviruses. The lentiviral supernatants were then collected after 48 h. The cells were infected with lentiviruses for 24 h and selected with puromycin.

Immunoprecipitation and western blotting

Immunoprecipitation was performed as described previously.[46] Briefly, cells were lysed on ice with NP-40 lysis buffer (150 mM NaCl, 100 mM NaF, 50 mM Tris-HCl (pH 7.6), 0.5% Nonidet P-40 (NP-40) and 1 mM PMSF) containing protease inhibitors and phosphatase inhibitors. Cell lysates were incubated with primary antibody and protein G-Sepharose beads for 3 h. The immunoprecipitants were washed three times with NP-40 lysis buffer and then subjected to western blot analysis.

For western blots, cell lysates were boiled in SDS loading buffer for 10 min, separated by SDS-PAGE, and then transferred to PVDF membranes (Millipore, Germany). The membranes were incubated with primary antibody and the corresponding secondary antibodies. Enhanced chemiluminescence (NCM Biotech, Suzhou, China) was used to detect the immunoreactive substrates. Chemiluminescence was detected using Azure Biosystem C300 (Azure, USA).

In western blot experiments, relative expression levels of α-SMA, COL1A1, p-Smad2 and p-Smad3 were quantified by reading the band intensity normalized against Tubulin. In Co-IP assays, relative immunoprecipitation level of different protein were quantified by reading the band intensity normalized against input.

Quantitative reverse transcription PCR

Cells were harvested and total RNA was extracted using a Trizol kit (Invitrogen). The cDNA was made by a reverse transcription kit (Tiangen, Beijing, China) and was used as the template for amplification. The level of β-actin was used as a normalization control. Quantitative PCR was carried out using GoTaq® qPCR Master Mix, according to the manufacturer's instructions.

The following primer sequences were used for quantitative reverse transcription PCR (5'-3'):

Human β-actin: forward, CAGCCTTCCTTCCTGGGCATG;
                reverse, ATTGTGCTGGGTGCCAGGGCAG;
Human Smad3: forward, TGGACGCAGGTTCTCCAAAC
                reverse, CCGGCTCGCAGTAGGTAAC
Human CXCL10: forward, GTGGCATTCAAGGAGTACCTC
                reverse, TGATGGCCTTCGATTCTGGATT
Human CCL2: forward, TCAAACTGAAGCTCGCACTCT
                reverse, GCATTGATTGCATCTGGCTG
Human IL-6: forward, TGCAATAACCACCCCTGACC
                reverse, GTGCCCATGCTACATTTGCC
Human IL-8: forward, TGGCAGCCTTCCTGATTTCT
                reverse, AATTTCTGTGTTGGCGCAGTG
Mouse CXCL10: forward, CCAAGTGCTGCCGTCATTTTC
                reverse, GGCTCGCAGGGATGATTTCAA
Mouse CCL2: forward, CACTCACCTGCTGCTACTCA
                reverse, GCTTGGTGACAAAAACTACAGC
Mouse IL-6: forward, ACAAGTCCGGAGAGGAGACT
                reverse, AATTGCCATTGCACAACTCTT
Human IL-8: forward, ACACTGCGCCAACACAGAAA
                reverse, CAACCCTCTGCACCCAGTTT

Chromatin immunoprecipitation (ChIP) assay

ChIP assay was performed as described previously.[47] HFL-1 cells were crosslinked by 1% formaldehyde for 10 min at room temperature. After washing for three times with ice-cold PBS, cells were detached from culture dish with cell lifter and lysed in SDS lysis buffer (1% SDS, 10 mM EDTA and 50 mM Tris (pH 8.1)) supplemented with protease inhibitors, and the chromatin was fragmented to 500–1000 bp with Bioruptor Plus sonication device (Diagenode, Switzerland). After centrifugation, soluble and diluted chromatin was incubated with primary antibodies or rabbit IgG overnight at 4°C, and the antibody-chromatin complexes were pulled down by protein G-Sepharose beads. The immunoprecipitants were washed, eluted, and then subjected to crosslink reversal and proteinase K treatment. The immunoprecipitated DNA was purified by a DNA purification kit (Axygen, Shanghai, China) and analyzed by quantitative PCR using primers against relevant promoters.

Primers used for ChIP-qPCR assay (5'-3'):

IL-6: forward, TCCCCCTAGTTGTGTCTTGC
           reverse, ATCTTTGTTGGAGGGTGAGGG
IL-8: forward, CCAGGAAGAAACCACCGGAA
           reverse, CAGGAAGGCTGCCAAGAGAG
CXCL10: forward, CTTGCCCGGCCCATAAAGTT
           reverse, GGGAACTAAGCTAATCTCAGGGA
CCL2: forward, TGGTCATGCCACAGGATGTC
           reverse, ATCCAGTCATGCTTCGGGTT

GST pull-down assay

GST or GST-tagged proteins were expressed in *E.coli* strain BL21 and purified using glutathione-sepharose (Sigma, Germany). His-tagged proteins were expressed in *E.coli* strain BL21 and purified using Ni-NTA agarose (Sigma, Germany). The glutathione-sepharose beads were incubated with GST or GST-tagged protein in 1 mL PBS at 4°C for 1 h. Unbound proteins were removed by washing with PBS for three times. The bead-bound GST or GST-tagged proteins were incubated with 500 ng His-tagged protein in 400 μL NP-40 lysis buffer (150 mM NaCl, 100 mM NaF, 50 mM Tris-HCl, pH 7.6, 0.5% Nonidet P-40 (NP-40) and 1 mM PMSF) at 4°C for 1 h. Unbound proteins were removed by washing with modified NP-40 lysis buffer for three times. The protein samples were boiled in loading buffer for 10 min for western blot analysis.

Immunohistochemistry and scoring

Mouse right lung was fixed with 4% formaldehyde before processing and paraffin embedding. The 5 μm sections were deparaffinized and rehydrated with xylene and different concentration of ethanol (100, 95, 80, 70, 50%). The sections were stained with hematoxylin and eosin for lung injury evaluation and Sirius red for fibrosis detection. Ashcroft scoring was used to assess pulmonary fibrosis and was carried out by averaging the scores from blinded scorer.

Immunofluorescence

HFL-1 cells were fixed in 4% formaldehyde and blocked with blocking buffer (3% BSA and 0.2% Triton X-100 in PBS). The cells were incubated with the primary antibodies overnight at 4°C, washed with washing buffer (0.2% BSA and 0.05% Triton X-100 in PBS) for three times, and incubated with secondary antibodies for 1 h at room temperature in the dark. The nuclei were stained with DAPI for 10 min. Image was captured with Zeiss LSM 780 confocal microscope (Zeiss, Germany).

Transwell chemotaxis assay

HFL-1 cells were seeded in 24 wells plate and transfected with plasmids for 12 h. The cell medium was replaced with serum-free Ham's F12 and cultured for another 24 h. THP-1 macrophage (5×10^4 cells) were seeded in upper chambers of transwell. After incubation for 16 h, non-migrated cells were removed by cotton swabs, and cells at another sides of chambers were stained with crystal violet.

Analysis of cytokines production

Cells were cultured for 24 h, then cell medium was replaced with serum-free Ham's F12 and cultured for another 24 h. Medium was collected and analyzed by human inflammation array C3 kit (AAH-INF-3) from RayBiotech (Atlanta, GA, USA). Chemiluminescence was detected using Azure Biosystem C300 (Azure, USA).

Collagen detection

Collagen secreted by cells was detected with Sirius Red Total Collagen Detection kit (Chondrex, USA). Culture medium was collected and concentrated with concentrating solution. After incubated at 4°C for 16 h, samples were centrifuged at 10,000 rpm for 3 min. Acetic acid was added to a concentration of 0.05M to dissolve the pellet for incubation with Sirius red solution. The samples were treated with washing solution and dissolved with extraction buffer before being transferred to 96-well plate and measured by TECAN spark reader (TECAN, Switzerland) at 530 nm.

ITC assay

Isothermal Titration Calorimetry (ITC) assay was performed with the microcal iTC200 (Malvern, UK). After washing with deionized water, 400 μL of GST-Smad3 (20 μM) and RMY-205 (0.2 mM) was loaded into the sample cell and injector. RMY-205 was then titrated stepwise into the Smad3 solution. PBS was used as the control. Data of heat changes were analyzed by microcal analysis launcher software.

Luciferase assay

Cells were transfected with CAGA luciferase reporter gene (a Smad3/4-dependent reporter), a β-galactosidase (β-gal) expression vectors and other relevant plasmids. At 24 hours after transfection, cells were lysed and measured for luciferase and β-gal activities. The β-gal activity was used to normalize the transfection efficiency.

Construction of recombinant adeno-associated virus

Adeno-associated virus (AAV) vector plasmids and two helper plasmids were transfected into 293T cells. After transfection for 72 h, 1/5 volume of PEG solution (40% PEG8000, 2.5 M NaCl, adding H_2O to 1 L) were added to culture medium and kept at 4°C overnight. The medium was centrifuged at 5,000 rpm for 5 min. The precipitates containing AAV were resuspended with PBS and subjected to Iodixanol gradients centrifugation. AAV was harvested in the 40% iodixanol fraction. The AAV fraction was transferred into a 100 K centrifugal filter to remove the iodixanol. The virus titer was determined by RT-PCR.

ELISA assay

Bronchoalveolar lavage fluid (BALF) was collected from AAV administration mice by lavage with 1 mL PBS. BALF was centrifuged at 300 g for 15 min and the supernatants were collected for ELISA. The culture medium from mouse primary pulmonary fibroblasts was centrifuged at 300 g for 15 min and the supernatants were collected for ELISA measurement. Levels of cytokines and chemokines were measured with ELISA kit (Abclonal, China) according to manufacturer's instruction.

Isolation of mouse primary pulmonary fibroblasts, BMDMs and neutrophils

Mouse primary pulmonary fibroblast, BMDMs and neutrophil isolation assays were performed as previously described.[48] Briefly, mice were sacrificed and cleaned with 75% alcohol, the chest was opened and the lung was removed. The lung was rinsed with sterile PBS and cut into 1 mm^3 pieces. The minced tissue was placed with forceps on 100 mm petri dish, and 10 mL of culture medium were gently added. The medium was changed every 2 days. After one week, the cells were detached with trypsin and passaged. For bone marrow-derived macrophages (BMDMs), tibias were collected from mice and bone marrow cells were flushed with DMEM medium. The bone marrow cell suspension was treated with red blood cell lysis buffer and filtered through 40 μm cell strainer. The single-cells were seeded in DMEM with 25% medium conditioned by L929 mouse fibroblasts and cultured for another 8 days. The mouse primary neutrophils from bone marrow were isolated by Percoll (Sigma, Germany) density gradient centrifugation (52%, 64%, and 72%) at 1,545 g for 30 min at room temperature. The interface between the 64% and 72% layers were collected as neutrophils.

Crosslinking assay

Cells were lysed in lysis buffer (12.5 mM HEPES (pH 7.5), 30 mM NaCl, 90 mM NaSCN, 1% NP-40) and centrifuged. Cell suspension were crosslinked with or without 1mM DSS for 10 min at room temperature. Crosslinking was terminated by adding 1 M Tris-HCl (pH 7.4) to a final concentration of 50 mM. After crosslinking, samples were subjected to immunoprecipitation using anti-Flag antibodies, follow by subjected to SDS-PAGE and analyzed by western blot.

Subcellular fractionation

Subcellular fractionation was performed as previously described.[49] Briefly, the cells were scratched from culture dish, washed once with cold PBS, and then lysed in 0.5 mL of NP-40 lysis buffer (10 mM HEPES (pH 7.9), 10 mM KCl, 0. 15% NP-40, 0.1 mM EDTA (pH 8.0), 0.1 mM EGTA and protease inhibitors). The cell lysates were centrifuged at 3,000 g for 5 min. The supernatant (cytoplasmic fraction) was collected. The pellet containing the nuclei was washed three times with 1 mL NP-40 lysis buffer, and resuspended in SDS lysis buffer (50 mM Tris-HCl (pH 8.0), 10 mM EDTA ,1% SDS and protease inhibitors) for sonication to obtain the nuclear fraction.

The SAR analysis of RMY-205 derivatives

To study the structure-activity relationships (SAR) of RMY-205, a series of RMY-205 derivatives were designed and synthesized as indicated in Table 2. All compounds were dissolved in DMSO and stored at −20°C.

Determination of EC$_{50}$

For the determination of EC$_{50}$ values, cells were transfected with CAGA luciferase reporter gene, β-gal expression vectors and other relevant plasmids. After transfection, cells were incubated with various concentrations of each compound for another 24 hours. Cells were lysed and measured for luciferase and β-gal activities. The EC$_{50}$ values were calculated using a dose-response model in GraphPad Prism 8.0 software.

Detection of RMY-205 pharmacokinetic (PK) properties

RMY-205 content in plasma was assayed at Truway Biotechnology Inc (Suzhou, China). Briefly, ICR mice (male, 8 weeks old) were administrated with a single dose of 2 mg/kg (intravenous injection (i.v.)), 10 mg/kg (intraperitoneal injection (i.p.) or oral gavage (p.o.)). Blood samples were collected at 5 min, 15 min, 30 min, 1 h, 2 h, 4 h, 8 h, and 24 h, respectively, and prepared by centrifugation of whole blood for 10 min at 1,500g. Subsequently, the plasma RMY-205 concentrations were determined by liquid chromatography-tandem mass spectrometry (LC-MS/MS), and the PK parameters were calculated using Phoenix WinNonlin 7.0.ZT-1a.

The synthesis of compound RMY-205
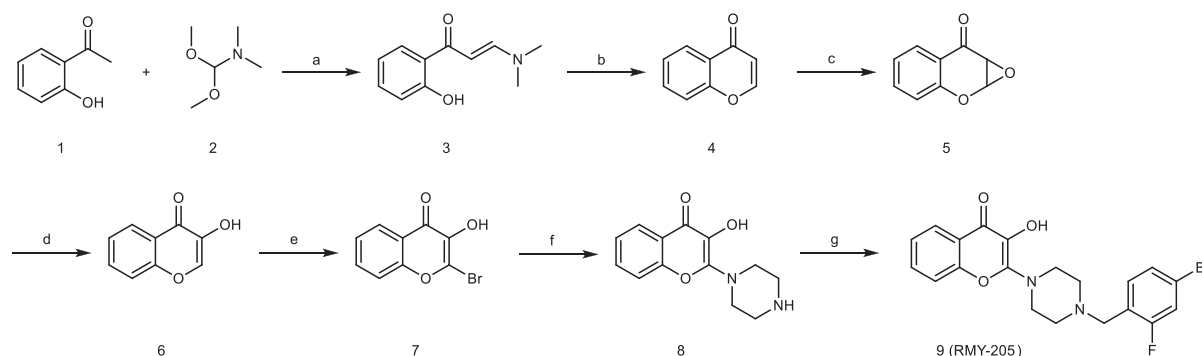
The synthesis route of compound RMY-205 (2-(4-(4-Bromo-2-fluorobenzyl)-piperazin-1-yl)-3-hydroxy-4H-chromen-4-one) was shown above. First, the active hydrogen at the α position of the carbonyl group of O-hydroxyacetophenone was reacted with the acetal, and the resulting α, β unsaturated carbonyl compounds (intermediate 3) were directly cyclized under strong acid conditions to form the chromanone parent structure (intermediate 4). The chromogens were oxidized to epoxy structure by H$_2$O$_2$ under the condition of strong base NaOH, and then hydrolyzed under strong acidic conditions to introduce hydroxyl groups to obtain chromogens substituted with hydroxyl group at position 3 (intermediate 6). The compound underwent a free radical reaction with NBS to introduce the bromine atom into position 2 (intermediate 7), and then inserting piperazine (intermediate 8). After introducing substituted benzyl group, target compound was finally obtained. All reactions were monitored by thin layer chromatography (TLC), and the structure of target compound was confirmed by Mass spectra (MS), ^{1}H NMR and ^{13}C NMR spectra.

Purification by column chromatography on silica gel (petroleum ether/ethyl acetate 1:0 → 1:1) gave product RMY-205 as a white solid. ^{1}H NMR (600 MHz, CDCl$_3$) δ 8.12 (dd, J = 7.9, 1.1 Hz, 1H), 7.52 – 7.49 (m, 1H), 7.33 (t, J = 7.6 Hz, 1H), 7.31 – 7.30 (m, 1H), 7.27 (d, J = 5.5 Hz, 2H), 7.22 (d, J = 9.9 Hz, 1H), 3.81 – 3.80 (m, 4H), 3.58 (s, 2H), 2.61 – 2.59 (m, 4H). ^{13}C NMR (151 MHz, CDCl$_3$) δ 169.94,

162.20, 160.53, 152.16, 150.30, 132.79, 131.50, 127.59, 125.24, 124.83, 124.69, 121.21, 119.36, 119.19, 116.75, 54.99, 52.85, 46.35. HRMS (ESI) m/z calcd for $C_{20}H_{18}BrFN_2O_3$ (M + H)$^+$ 433.0563; found, 433.0561.

NMR ans MS data for RMY-205 derivatives

All the derivatives of RMY-205 was synthesized according to the same procedure of RMY-205.

Compound RMY-189: ^{1}H NMR (600 MHz, CDCl$_3$) δ 8.13 - 8.17 (m, 1 H), 7.49 - 7.53 (m, 1 H), 7.30 - 7.35 (m, 6 H), 7.28 (td, *J*=5.8, 2.8 Hz, 1 H), 3.79 - 3.88 (m, 4 H), 3.57 (s, 2 H), 2.60 (t, *J*=4.9 Hz, 4 H). ^{13}C NMR (151 MHz, CDCl$_3$) δ 169.7, 151.9, 150.3, 137.6, 131.2, 129.2, 128.3, 127.3, 125.0, 124.6, 124.4, 121.1, 116.5, 63.0, 53.0, 46.3. HRMS (ESI) m/z calcd for $C_{20}H_{20}N_2O_3$ [M+H]$^+$ 337.1547, found 337.1545.

Compound RMY-188: ^{1}H NMR (600 MHz, CDCl$_3$) δ 8.15 (dd, *J*=7.8, 1.2 Hz, 1 H), 7.49 - 7.54 (m, 1 H), 7.37 - 7.42 (m, 1 H), 7.29 - 7.36 (m, 2 H), 7.25 - 7.28 (m, 1 H), 7.13 (t, *J*=7.4 Hz, 1 H), 7.05 (t, *J*=9.1 Hz, 1 H), 3.79 - 3.90 (m, 4 H), 3.66 (s, 2 H), 2.59 - 2.69 (m, 4 H). ^{13}C NMR (151 MHz, CDCl$_3$) δ 169.7, 162.3, 160.6, 151.9, 150.3, 131.6, 131.6, 131.2, 129.1, 129.1, 125.0, 124.6, 124.4, 124.1, 124.0, 124.0, 123.9, 121.1, 116.5, 115.5, 115.3, 55.3, 52.7, 46.2. HRMS (ESI) m/z calcd for $C_{20}H_{19}FN_2O_3$ [M+H]$^+$ 355.1452, found 355.1448.

Compound RMY-183: ^{1}H NMR (600 MHz, CDCl$_3$) δ 8.15 (d, *J*=7.7 Hz, 1 H), 7.47 - 7.57 (m, 2 H), 7.29 - 7.40 (m, 3 H), 7.25 - 7.27 (m, 1 H), 7.19 - 7.23 (m, 1 H), 3.78 - 3.92 (m, 4 H), 3.69 (s, 2 H), 2.64 - 2.71 (m, 4 H). ^{13}C NMR (151 MHz, CDCl$_3$) δ 169.7, 151.9, 150.3, 135.3, 134.5, 131.2, 130.8, 129.6, 128.4, 126.7, 125.0, 124.7, 124.4, 121.1, 116.5, 59.2, 53.0, 46.3. HRMS (ESI) m/z calcd for $C_{20}H_{19}ClN_2O_3$ [M+H]$^+$ 371.1157, found 371.1146.

Compound WBR-14: ^{1}H NMR (600 MHz, CDCl$_3$) δ 8.15 (dd, *J*=7.9, 1.5 Hz, 1 H), 7.68 (d, *J*=7.7 Hz, 1 H), 7.57 - 7.60 (m, 1 H), 7.54 - 7.57 (m, 1 H), 7.51 - 7.54 (m, 1 H), 7.37 - 7.41 (m, 1 H), 7.30 - 7.37 (m, 2 H), 3.81 - 3.88 (m, 4 H), 3.77 (s, 2 H), 2.65 - 2.70 (m, 4 H). ^{13}C NMR (151 MHz, CDCl$_3$) δ 169.8, 152.0, 150.2, 141.8, 133.1, 132.6, 131.3, 130.1, 127.9, 125.0, 124.7, 124.5, 121.0, 117.8, 116.6, 113.2, 60.5, 52.8, 46.2. HRMS (ESI) m/z calcd for $C_{21}H_{19}N_3O_3$ [M+H]$^+$ 362.1499, found 362.1494.

Compound WBR-10: ^{1}H NMR (600 MHz, CDCl$_3$) δ 8.15 (dd, *J*=7.9, 1.5 Hz, 1 H), 7.50 - 7.54 (m, 1 H), 7.34 (t, *J*=7.6 Hz, 1 H), 7.32 (d, *J*=8.8 Hz, 1 H), 7.27 - 7.30 (m, 1 H), 7.09 - 7.13 (m, 2 H), 6.97 (td, *J*=8.4, 1.9 Hz, 1 H), 3.81 - 3.89 (m, 4 H), 3.58 (s, 2 H), 2.59 - 2.65 (m, 4 H). ^{13}C NMR (151 MHz, CDCl$_3$) δ 169.7, 163.8, 162.2, 151.9, 150.4, 140.2, 140.2, 131.3, 129.8, 129.8, 125.0, 124.7, 124.6, 124.6, 124.5, 121.1, 116.5, 115.9, 115.7, 114.3, 114.2, 62.3, 52.9, 46.2. HRMS (ESI) m/z calcd for $C_{20}H_{19}FN_2O_3$ [M+H]$^+$ 355.1452, found 355.1449.

Compound WBR-12: ^{1}H NMR (600 MHz, CDCl$_3$) δ 8.15 (dd, *J*=7.9, 1.3 Hz, 1 H), 7.51 - 7.54 (m, 1 H), 7.37 (s, 1 H), 7.35 (d, *J*=7.3 Hz, 1 H), 7.31 - 7.34 (m, 1 H), 7.25 - 7.27 (m, 2 H), 7.21 - 7.24 (m, 1 H), 3.81 - 3.89 (m, 4 H), 3.55 (s, 2 H), 2.57 - 2.67 (m, 4 H). ^{13}C NMR (151 MHz, CDCl$_3$) δ 169.7, 151.9, 150.4, 139.7, 134.3, 131.3, 129.6, 129.1, 127.6, 127.2, 125.0, 124.7, 124.5, 121.1, 116.5, 62.3, 52.9, 46.2. HRMS (ESI) m/z calcd for $C_{20}H_{19}ClN_2O_3$ [M+H]$^+$ 371.1157, found 371.1154.

Compound RMY-186: ^{1}H NMR (600 MHz, CDCl$_3$) δ 8.15 (dd, *J*=7.9, 1.1 Hz, 1 H), 7.49 - 7.56 (m, 2 H), 7.41 (d, *J*=7.9 Hz, 1 H), 7.30 - 7.36 (m, 2 H), 7.26 - 7.29 (m, 1 H), 7.18 - 7.22 (m, 1 H), 3.75 - 3.90 (m, 4 H), 3.53 (s, 2 H), 2.59 (t, *J*=4.9 Hz, 4 H). ^{13}C NMR (151 MHz, CDCl$_3$) δ 169.7, 151.9, 150.3, 140.2, 132.0, 131.2, 130.4, 129.9, 127.6, 125.0, 124.7, 124.4, 122.6, 121.1, 116.5, 62.3, 52.9, 46.2. HRMS (ESI) m/z calcd for $C_{20}H_{19}BrN_2O_3$ [M+H]$^+$ 415.0652, found 415.0655.

Compound WBR-11: ^{1}H NMR (600 MHz, CDCl$_3$) δ 8.15 (dd, *J*=7.9, 1.5 Hz, 1 H), 7.53 (ddd, *J*=8.5, 7.1, 1.7 Hz, 1 H), 7.35 (t, *J*=7.6 Hz, 1 H), 7.33 (s, 1 H), 7.30 - 7.32 (m, 2 H), 7.01 - 7.04 (m, 2 H), 3.80 - 3.89 (m, 4 H), 3.56 (s, 2 H), 2.58 - 2.64 (m, 4 H). ^{13}C NMR (151 MHz, CDCl$_3$) δ 169.7, 163.0, 161.4, 151.9, 150.4, 132.9, 131.3, 130.8, 130.7, 125.0, 124.7, 124.5, 121.1, 116.5, 115.3, 115.2, 62.1, 52.8, 46.1. HRMS (ESI) m/z calcd for $C_{20}H_{19}FN_2O_3$ [M+H]$^+$ 355.1452, found 355.1440.

Compound RMY-202: ^{1}H NMR (600 MHz, CDCl$_3$) δ 8.15 (d, *J*=7.9 Hz, 1 H), 7.52 (t, *J*=7.7 Hz, 1 H), 7.27 - 7.36 (m, 6 H), 3.77 - 3.89 (m, 4 H), 3.53 (s, 2 H), 2.53 - 2.63 (m, 4 H). ^{13}C NMR (151 MHz, CDCl$_3$) δ 169.7, 151.9, 150.3, 136.2, 133.0, 131.2, 130.4, 128.5, 125.0, 124.7, 124.4, 121.1, 116.5, 62.2, 52.9, 46.2. HRMS (ESI) m/z calcd for $C_{20}H_{19}ClN_2O_3$ [M+H]$^+$ 371.1157, found 371.1154.

Compound RMY-190: ^{1}H NMR (600 MHz, CDCl$_3$) δ 8.15 (d, *J*=7.7 Hz, 1 H), 7.49 - 7.54 (m, 1 H), 7.46 (m, *J*=8.3 Hz, 2 H), 7.30 - 7.36 (m, 2 H), 7.23 (m, *J*=8.3 Hz, 2 H), 3.80 - 3.85 (m, 4 H), 3.51 (s, 2 H), 2.58 (t, *J*=4.8 Hz, 4 H). ^{13}C NMR (151 MHz, CDCl$_3$) δ 169.7, 151.9, 150.3, 136.7, 131.5, 131.2, 130.8, 125.0, 124.7, 124.4, 121.1, 121.1, 116.5, 62.2, 52.9, 46.2. HRMS (ESI) m/z calcd for $C_{20}H_{19}BrN_2O_3$ [M+H]$^+$ 415.0652, found 415.0652.

Compound WBR-9: ^{1}H NMR (600 MHz, CDCl$_3$) δ 8.14 (dd, *J*=7.9, 1.5 Hz, 1 H), 7.48 - 7.53 (m, 1 H), 7.29 - 7.35 (m, 2 H), 7.24 - 7.27 (m, 1 H), 6.88 - 6.93 (m, 2 H), 3.80 - 3.91 (m, 4 H), 3.78 (s, 2 H), 2.67 (t, *J*=4.8 Hz, 4 H). ^{13}C NMR (151 MHz, CDCl$_3$) δ 169.6, 162.9, 162.8, 161.3, 161.2, 151.9, 150.3, 131.2, 129.6, 129.6, 129.5, 125.0, 124.6, 124.4, 121.1, 116.5, 112.2, 111.3, 111.3, 111.2, 111.1, 52.0, 48.6, 46.2. HRMS (ESI) m/z calcd for $C_{20}H_{18}F_2N_2O_3$ [M+H]$^+$ 373.1358, found 373.1348.

Compound RMY-195: ^{1}H NMR (600 MHz, CDCl$_3$) δ 8.15 (dd, *J*=7.9, 1.3 Hz, 1 H), 7.49 - 7.54 (m, 1 H), 7.30 - 7.36 (m, 2 H), 7.21 (dd, *J*=8.3, 6.2 Hz, 1 H), 6.89 (dd, *J*=9.7, 2.4 Hz, 1 H), 6.81 - 6.86 (m, 1 H), 3.80 (br. s, 4 H), 3.47 (s, 2 H), 2.57 (t, *J*=4.9 Hz, 4 H), 2.38 (s, 3 H). ^{13}C NMR (151 MHz, CDCl$_3$) δ 169.7, 162.8, 161.2, 151.9, 150.4, 140.0, 140.0, 131.5, 131.5, 131.4, 131.3, 131.2, 125.0, 124.7, 124.4, 121.1, 117.1, 117.0, 116.5, 112.1, 112.0, 60.2, 52.9, 46.4, 19.4. HRMS (ESI) m/z calcd for $C_{21}H_{21}FN_2O_3$ [M+H]$^+$ 369.1609, found 369.1608.

Compound WBR-1: ^{1}H NMR (600 MHz, CDCl$_3$) δ 7.71 (dd, *J*=8.3, 2.9 Hz, 1 H), 7.39 - 7.41 (m, 1 H), 7.33 (d, *J*=8.3 Hz, 1 H), 7.24 (dd, *J*=9.2, 4.0 Hz, 1 H), 7.16 (td, *J*=8.4, 3.0 Hz, 1 H), 7.10 - 7.13 (m, 1 H), 3.73 - 3.80 (m, 4 H), 3.44 (s, 2 H), 2.52 (t, *J*=4.9 Hz, 4 H). ^{13}C NMR (151 MHz, CDCl$_3$) δ 168.8, 160.1, 158.5, 150.6, 148.0, 138.1, 132.5, 131.3, 130.8, 130.4, 128.3, 124.7, 122.4, 122.4, 119.3, 119.1, 118.4, 118.4, 110.2, 110.0, 61.7, 52.9, 46.3. HRMS (ESI) m/z calcd for $C_{20}H_{17}Cl_2FN_2O_3$ [M+H]$^+$ 423.0673, found 423.0673.

Compound WBR-2: ^{1}H NMR (600 MHz, CDCl$_3$) δ 7.71 (dd, *J*=8.3, 2.9 Hz, 1 H), 7.37 (d, *J*=8.8 Hz, 1 H), 7.24 (dd, *J*=9.0, 4.0 Hz, 1 H), 7.14 - 7.18 (m, 1 H), 7.01 (d, *J*=3.1 Hz, 1 H), 6.64 (dd, *J*=8.8, 3.1 Hz, 1 H), 3.76 - 3.81 (m, 4 H), 3.74 (s, 3 H), 3.56 (s, 2 H), 2.58 - 2.63 (m, 4 H). ^{13}C NMR (151 MHz, CDCl$_3$) δ 168.7, 160.1, 159.0, 158.5, 150.6, 148.0, 138.0, 133.4, 124.7, 122.4, 122.4, 119.2, 119.0, 118.4, 118.3, 116.5, 115.0, 114.2, 110.1, 110.0, 61.7, 55.5, 53.0, 46.4. HRMS (ESI) m/z calcd for C$_{21}$H$_{20}$BrFN$_2$O$_4$ [M+H]$^+$ 463.0663, found 463.0664.

Compound WBR-5: ^{1}H NMR (600 MHz, CDCl$_3$) δ 8.26 (d, *J*=2.4 Hz, 1 H), 7.58 (dd, *J*=8.8, 2.4 Hz, 1 H), 7.46 (d, *J*=1.8 Hz, 1 H), 7.40 (d, *J*=8.1 Hz, 1 H), 7.17 - 7.22 (m, 2 H), 3.82 - 3.86 (m, 4 H), 3.51 (s, 2 H), 2.59 (t, *J*=5.0 Hz, 4 H). ^{13}C NMR (151 MHz, CDCl$_3$) δ 168.3, 150.6, 150.5, 138.1, 134.0, 132.5, 131.2, 130.8, 130.3, 128.3, 127.6, 124.9, 122.7, 118.3, 117.7, 61.7, 52.9, 46.3. HRMS (ESI) m/z calcd for C$_{20}$H$_{17}$BrCl$_2$N$_2$O$_3$ [M+H]$^+$ 482.9872, found 482.9875.

Compound WBR-6: ^{1}H NMR (600 MHz, CDCl$_3$) δ 8.27 (d, *J*=2.4 Hz, 1 H), 7.58 (dd, *J*=8.8, 2.4 Hz, 1 H), 7.44 (d, *J*=8.8 Hz, 1 H), 7.20 (d, *J*=8.8 Hz, 1 H), 7.08 (d, *J*=3.1 Hz, 1 H), 6.71 (dd, *J*=8.8, 3.1 Hz, 1 H), 3.84 - 3.87 (m, 4 H), 3.81 (s, 3 H), 3.62 (s, 2 H), 2.67 - 2.69 (m, 4 H). ^{13}C NMR (151 MHz, CDCl$_3$) δ 168.2, 159.0, 150.6, 150.5, 138.0, 134.0, 133.3, 127.6, 124.8, 122.7, 118.3, 117.7, 116.4, 115.0, 114.1, 61.7, 55.5, 52.9, 46.4. HRMS (ESI) m/z calcd for C$_{21}$H$_{20}$Br$_2$N$_2$O$_4$ [M+H]$^+$ 522.9863, found 522.9865.

QUANTIFICATION AND STATISTICAL ANALYSIS

For the western blot, all the experiments were repeated at least twice, and one of the representative western blot results was shown, in which the intensities of electrophoresis bands relative to the loading control (such as Tubulin) were quantified and shown under each band. For other results with bar graphs, the statistical analysis is carried out based on at least three independent experiments. The data are expressed as the mean ± SEM, and the statistical analysis of differences between two groups was performed by using two-tailed Student's t-test. The differences between multiple groups were analyzed by using one-way or two-way ANOVA, followed by Tukey's post hoc test. The statistical analysis was performed by using GraphPad Prism 8. *$p < 0.05$ was considered statistically significant, **$p < 0.01$ was considered highly significant, and ***$p < 0.001$ was considered extremely significant. NS, not significant.